Dipole transitions to bound states in ^{56}Fe and ^{58}Ni

F. Bauwens,[1] J. Bryssinck,[1] D. De Frenne,[1] K. Govaert,[1] L. Govor,[2] M. Hagemann,[1] J. Heyse,[1] E. Jacobs,[1] W. Mondelaers,[1] and V. Yu. Ponomarev[1,*]

[1]*Vakgroep Subatomaire en Stralingsfysica, Proeftuinstraat 86, 9000 Gent, Belgium*

[2]*Russian Scientific Centre Kurchatov Institute, Moscow, Russia*

(Received 2 February 2000; published 23 June 2000)

A high-resolution study of dipole transitions to bound states up to 10 MeV in the fp-shell nuclei ^{56}Fe and ^{58}Ni was performed by means of the nuclear resonance fluorescence method. Unpolarized and partially linearly polarized bremsstrahlung photons with different end point energies (6.5, 10, and 12 MeV) were used to determine excitation energies, spins, parities, and transition widths of more than 60 levels observed in each nucleus between 2 and 10 MeV. The vast majority of the observed transitions are dipole ones and to the strongest of them an $E1$ assignment could be given. The $E1$ strength distribution shows a high concentration around 8.2 MeV that may be connected with the $E1$ pygmy resonance in heavier nuclei. The $M1$ spin-flip strength shows a concentration around 8.7 MeV in ^{58}Ni. On the contrary, in ^{56}Fe its distribution is rather flat. The observed $M1$ strength is weak in both nuclei. A study was made of the feeding and branching of the observed levels. Calculations were performed for these nuclei in the framework of the quasiparticle phonon model and a comparison with experimental results is made. Apart from the strength, experimental and calculated results agree quite well and information about a scissorslike mode in ^{56}Fe and a 1^- two-phonon state in ^{58}Ni could be extracted.

PACS number(s): 23.20.Lv, 25.20.Dc, 27.40.+z

I. INTRODUCTION

Recently the study of electric dipole transitions from high-lying bound states in nuclei gained much interest. The $E1$ strength distribution in spherical nuclei near shell closures seems to display quite some fine structure in this energy region and modulations of the giant dipole resonance (GDR) tail occur. Lately, experimental efforts have been made on ^{116,124}Sn [1], ^{138}Ba [2], ^{140}Ce [3], and the odd ^{89}Y [4], using the photon scattering technique. A conspicuous concentration of $E1$ strength turned up clearly around 6.5 MeV in these nuclei. This ''pygmy resonance,'' named as such in analogy to the GDR, was first observed in heavier nuclei in the Pb region [5] at 5.5 MeV. Indications of its presence in Ba and Ce isotopes [6] and in the $N=50$ nuclei ^{88}Sr and ^{90}Zr [7–9] were also found. For ^{92}Mo a recent photon scattering experiment at the 15 MeV linac in Gent established the presence and the $E1$ character of this pygmy resonance centered at 6.5 MeV [10]. Theoretically, this local increase of $E1$ strength can be explained in different ways. It was reproduced by Oros *et al.* using a two-group schematic random phase approximation (RPA) model, suggesting that between the unperturbed $1p$-$1h$ states concentrations of strength remain when the rest of the strength is pulled up into the GDR [11]. A similar interpretation is given in a microscopic quasiparticle phonon model (QPM) in Refs. [1–3]. The observed position of the pygmy resonance in ^{116}Sn was nicely reproduced with this method. In a macroscopic way, it can be considered as an oscillation of a small part of the nuclear surface against the nucleus bulk [12,13]. Van Isacker *et al.* suggested that only part of the neutron skin is responsible for this phenomenon [14].

In an attempt to extend these $E1$ strength systematics further into the medium-heavy and light nuclei, we report here on a high-resolution study of dipole transitions below the neutron emission threshold in the fp-shell nuclei ^{56}Fe and ^{58}Ni. In addition, these nuclei, in the vicinity of the closed $N,Z=28$ shell, also represent a favorable region to observe spin-flip $M1$ resonances. In ^{56}Fe the neutron $1f_{7/2}$ shell is completely filled while the $1f_{5/2}$ orbitals are populated by two neutrons only. The proton $1f_{7/2}$ orbitals are almost completely filled except for two proton holes. In ^{58}Ni the two extra protons close the $1f_{7/2}$ shell. As the gap energy between these two orbitals is expected to be about 8 MeV, a considerable $M1$ strength, corresponding to $1f_{7/2}\rightarrow 1f_{5/2}$ spin-flip transitions, can be expected in this energy region. This was confirmed by electron and proton scattering experiments on these nuclei [15,16].

Because of the high selectivity of the photon probe, exciting nuclei mainly via dipole and to a much lesser extent via electric quadrupole transitions, nuclear resonance fluorescence (NRF) is a very effective method to study the above-mentioned dipole transitions. In the $M1$ spin-flip or pygmy resonance regions where the level density becomes quite high, this is an important asset. Combined with the excellent knowledge of the electromagnetic interaction and the use of high-resolution germanium detectors we can measure model independently decay widths Γ, parities, and spins of individual levels up to the particle emission energy. In the fp shell, the neutron separation energy is quite high, allowing one to map the dipole strength up to 10 MeV. It should be pointed out, however, that, although the NRF method represents an ideal tool to study $E1$ transitions, it is not as ideal for detecting $M1$ transitions as methods based on electrons or hadronic probes. Since we observe the deexcitation of levels, $E1$ branching from 1^+ states to 0^-, 1^-, or 2^- levels

*Permanent address: Bogoliubov Laboratory of Theoretical Physics, Joint Institute of Nuclear Research, Dubna, Russia.

(having higher probability than the direct $M1$ transition to the ground state) will cause the observed $M1$ strength to diminish. A comparison between QPM calculations and NRF experiments on Sn nuclei [1] revealed also that the heavy fragmentation of the $M1$ strength caused the cross sections of the individual transitions to fall below the detection limits. In the lighter fp-shell nuclei fragmentation will be less, so we expect to observe at least the strongest $M1$ transitions.

In ^{56}Fe(γ,γ') experiments performed by Kumagai *et al.* [17], Ishkanov *et al.* [18], and Chapuran *et al.* [19], several transitions have been identified between 3 and 10 MeV. In the latter and most extensive experiment, bremsstrahlung photons were used, produced at the 100% duty cycle MUSL-2 accelerator of the University of Illinois. About 46 transitions were observed in two runs with maximum energies of 7.6 and 10.3 MeV. Although excitation energies and transition width ratios Γ_0^2/Γ were obtained for 46 levels, spins were determined for only 13 excited states below 7.6 MeV. In a ^{56}Fe$(\vec{\gamma},\gamma')$ experiment performed in Giessen (see Ref. [9] and references therein) with off-axis polarized bremsstrahlung, the parity of eight levels could be determined. For seven of them a J^π value of 1^- was found while only for one level a J^π value of 1^+ was obtained. In a short test run with off-axis polarized bremsstrahlung at the then newly installed facility in Gent [20], intended to show the potential of the setup, the parities of nine levels in ^{56}Fe were obtained. The work presented here is partly the continuation of this ^{56}Fe$(\vec{\gamma},\gamma')$ experiment. It was intended to increase the statistical accuracy, allowing one to prove the expected presence of several $M1$ transitions and to study the $E1$ strength distribution. At the same time, to achieve a complete characterization of the observed transitions, spins for levels up to 10 MeV in ^{56}Fe were determined through measurements with unpolarized bremsstrahlung.

Almost 20 years ago, ^{58}Ni was studied at the NRF setup in Giessen. In (γ,γ') experiments [21], ten levels were observed and for five transitions the parity could be determined [22] using polarized bremsstrahlung. An extended survey of the $M1$ strength distribution, based on electron scattering experiments, already exists [15], but the $E1$ strength and its fragmentation below the neutron separation energy remains largely unknown. Our present investigation of the dipole response in ^{58}Ni extends this available information and allows at the same time for a precise and detailed comparison with the (e,e') work and with our results for ^{56}Fe.

II. EXPERIMENTAL SETUP AND PROCEDURE

A. NRF method and formalism

NRF experiments using a continuous energy photon beam from an intense bremsstrahlung source allow the simultaneous observation of all nuclear $J=1$ states in even-even nuclei that have a sufficiently high ground state transition width. By observing the photons from the deexcitation process with Ge detectors, the fragmentation of the dipole strength for energies up to the end point energy of the bremsstrahlung can be investigated.

The NRF method and the relevant features for the setup in Gent have been extensively reported on in, among others, Refs. [1,20,23–25]. We give here, based on these references, a short synopsis of the most important observables.

The photon scattering cross section integrated over a single resonance, is given by

$$\frac{d\sigma(\vec{\gamma},\gamma')}{d\Omega}=\frac{2J+1}{2J_0+1}\left(\frac{\pi\hbar c}{E_x}\right)^2\left(\frac{\Gamma_0\Gamma_i}{\Gamma}\right)\frac{W(\theta,\phi)}{4\pi}, \quad (1)$$

where J_0 and J are the spins of the ground and excited state, respectively. Γ_0, Γ_i, and Γ represent the ground state decay width, the decay width to an intermediate level, and the total decay width of the considered excited state. E_x is the excitation energy of the level and $W(\theta,\phi)$ the angular distribution of the emitted radiation. The scattering angle θ is the angle between the incoming and scattered photon, while the azimuthal angle ϕ is defined by the angle between the scattering and the polarization plane. For unpolarized bremsstrahlung, the angular distribution becomes dependent only on θ and can be described by a sum of Legendre polynomials, depending on the multipolarity of the transition [26]. Measuring $W(\theta)$ enables the determination of the multipolarity of the transition. For even-even nuclei with ground state spin $J_0=0$ it is sufficient to measure only under the optimal angles of 90° and 127°. The ratio $W(90°)/W(127°)$ amounts to 0.73 for dipole transitions and 2.28 for quadrupole transitions. The latter value is slightly changed to 2.14 when the solid angles of the detectors are taken into account. For elastic transitions, where the excited state decays back to the ground state ($\Gamma_i=\Gamma_0$), the observed cross section is proportional to Γ_0^2/Γ. If the total decay width is known, or assumed to equal the ground state transition width ($\Gamma\approx\Gamma_0$), the reduced transition probability $B(\pi,L)\uparrow$ for the transition with parity π and multipolarity L is extracted by means of the relation:

$$\Gamma_0=\frac{8\pi(L+1)}{L[(2L+1)!!]^2}\left(\frac{E_x}{\hbar c}\right)^{2L+1}\frac{2J_0+1}{2J+1}B(\pi,L)\uparrow. \quad (2)$$

Parities were determined using linearly polarized photons in the entrance channel and by measuring the azimuthal asymmetry of the scattered photons. The asymmetry is measured for photons scattered parallel ($\phi_\parallel=0°,180°$) and perpendicular ($\phi_\perp=90°,270°$) to the polarization plane under a scattering angle $\theta=90°$. The analyzing power $\Sigma(\theta)$ for this reaction is defined as the normalized difference of the angular distributions perpendicular ($\perp$) and parallel ($\parallel$) to the polarization plane:

$$\Sigma(\theta)=\frac{W(\theta,\phi=\phi_\perp)-W(\theta,\phi=\phi_\parallel)}{W(\theta,\phi=\phi_\perp)+W(\theta,\phi=\phi_\parallel)}. \quad (3)$$

The maximum analyzing power for 0-1-0 and 0-2-0 spin cascades occurs at $\theta=90°$ and is $+1$ for negative parity transitions ($E1$) and -1 for positive parity transitions ($M1$

TABLE I. Overview of the NRF experiments.

Nucleus	Reaction	$E_{\gamma,max}$ (MeV)	Target material	Measurement time (h)
^{56}Fe	(γ,γ')	10	1.5 g ^{nat}Fe+H_3BO_3	300
	(γ,γ')	6.5	1.5 g ^{nat}Fe+H_3BO_3	100
	$(\vec{\gamma},\gamma')$	12	10.5 and 13.8 g ^{nat}Fe	530
^{58}Ni	(γ,γ')	10	1.5 g ^{58}Ni (95.9%)+H_3BO_3	300
	(γ,γ')	6.5	1.5 g ^{58}Ni (95.9%)+H_3BO_3	100
	$(\vec{\gamma},\gamma')$	12	9.5 g ^{58}Ni (99.9%)	470

and $E2$) [27]. For a not completely polarized incoming beam with polarization P_γ, the measured asymmetry ϵ can be represented as

$$\epsilon = \frac{N_\perp - N_\parallel}{N_\perp + N_\parallel} = P_\gamma \Sigma(\theta), \tag{4}$$

where $N_\perp$ and $N_\parallel$ are the number of counts, respectively, for the detectors perpendicular to and in the polarization plane. Comparing the measured asymmetry with the known polarization degree of the beam thus reveals the parity of the observed transition.

B. Setup and procedure

Our NRF experiments were performed at the 15 MeV linac in Gent. The setup is described in detail in Ref. [20]. The experiments with unpolarized photons were performed with bremsstrahlung with end point energies of 10 and 6.5 MeV. The measurements with 6.5 MeV bremsstrahlung are necessary as the feeding of a level (caused by transitions from higher-lying levels) becomes important at about 4 MeV below the maximum bremsstrahlung energy [1,23]. By performing experiments with different maximum energies for the bremsstrahlung this feeding problem is circumvented and accurate transition strength information for energies between 2 MeV and 10 MeV is extracted. The feeding systematics can be studied and comparison between both measurements allows one to identify the branching behavior for several levels.

For the unpolarized measurements the targets consisted in both cases of thin metallic disks of about 2 cm diameter. Similar disks of boron acid (H_3BO_3) were alternately inserted between the iron or nickel disks. Table I displays the amounts used, the enrichment of the targets, and the effective measuring time per detector. Seven well-known strong transitions in ^{11}B [28] and ^{16}O [29] were used for energy and efficiency calibration. The energy calibration is not only important for determining the transition energies in the target nucleus, but also to enable for the correction of eventual shifts in the gain of the amplification chains of the detectors.

The efficiency calibration is especially important for determining the correct transition probabilities. The relation between the observed area A of a peak in the spectrum and the scattering cross section is

$$A = I_s N_t \epsilon N_\gamma W(\theta) \quad (\theta = 90°, 127°), \tag{5}$$

where I_s is the cross section integrated over the single resonance and over the full solid angle, N_t the number of target nuclei, ϵ the detector efficiency, and N_γ the photon flux. The quantity $\epsilon_N = N_t \epsilon N_\gamma$ is determined as a function of the photon energy using the measured areas, the known cross sections, and angular distributions for the transitions in the calibration material included in the target. In this way, the calibration and studied targets are measured simultaneously under exactly the same conditions; also the effects of solid angle and absorbers are included, and the need to perform separate measurements of the photon flux is avoided. Feeding effects in the calibration nuclei were measured in separate experiments using boron acid targets and are taken into account. To the experimental ϵ_N values a three-parameter least-squares fit of the form

$$\epsilon_N(E_x) = \exp(a_1 + a_2 E_x + a_3 E_x^2) S(E_x, E_e) \tag{6}$$

was performed, where $S(E_x, E_e)$ represents the thin target Schiff bremsstrahlung spectrum [30], depending on the bremsstrahlung end point energy E_e. Figure 1 displays $\epsilon_N(E_x)$ measured in the 10 MeV ^{58}Ni experiment (full energy and escape lines are included).

The experiments with polarized photons were performed with bremsstrahlung with an end point energy of 12 MeV. Since the polarization degree P_γ of the beam drops to zero near the end point energy, we can only start determining

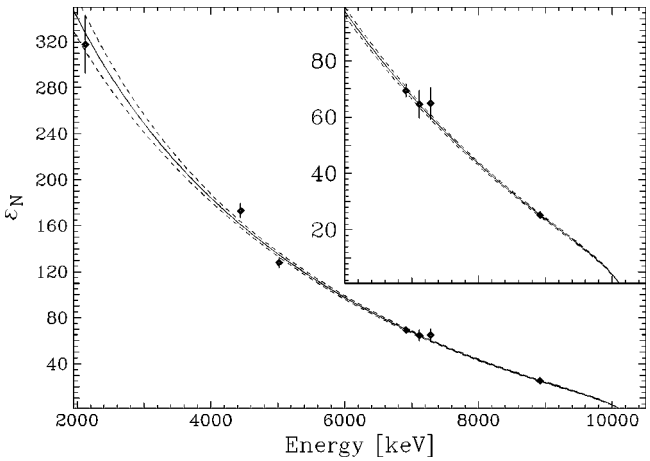

FIG. 1. $\epsilon_N(E_x)$ at $\theta = 127°$ as a function of the excitation energy (taking full energy and escape lines into account) for the 10 MeV ^{58}Ni experiment. The meaning of ϵ_N is explained in the text.

meaningful asymmetries about 2 MeV below this energy. Parities can, with only a few exceptions, be determined from 6 MeV up to 10 MeV. At the very low energies P_γ is high enough, but as a result of the worse peak-to-background ratio and the feeding mechanism, which destroys the azimuthal asymmetry, it becomes in general impossible to determine parities.

The targets were of the same shape as in the experiments with unpolarized photons. Details are given in Table I. In the case of ^{56}Fe the spectrum results from two separate experimental runs with slightly different amounts of target material. The strongly enriched ^{58}Ni target had a powdery form and was contained in a thin disk-shaped polyethylene packing. The four Ge detectors were arranged at a scattering angle of 90° and azimuthal angles of 0°, 90°, 180°, and 270°. Since the quality of these spectra is lower than those recorded with unpolarized photons, we used them only for parity determination and not to extract transition strengths. Therefore the targets contained no H_3BO_3 standard.

Uncertainties include mainly statistical errors. For each angle, the γ energies were corrected for Doppler and recoil effects to obtain the right level excitation energy. Where possible, the weighted average over the full energy, single escape, and double escape lines was taken. In the uncertainties in the energy, a contribution stemming from the polynomial fit through the calibration standard data points was added linearly for each energy and angle. The final energies are the weighted average over the two angles. For the cross sections only statistical uncertainties were taken into account. Since a direct determination of the photon flux was not necessary with our method, the most important factor is the uncertainty in the peak areas. The uncertainty in ϵ_N contributes mainly at high energies or for the strongest transitions. No correction for nuclear or atomic self-absorption was necessary, since the amounts of target material were rather small. The main source of systematical errors originates from the feeding effect, which we will discuss later.

III. RESULTS

Figures 2 and 3 display the high-energy part of the (γ,γ') spectra of ^{56}Fe and ^{58}Ni for $E_{\gamma,max}=6.5$ and 10 MeV, taken at 127°. The H_3BO_3 calibration lines are indicated with arrows. Because of the appearance, for each transition, of full energy, single escape, and double escape lines, the spectra at 10 MeV are rather complex, but because of the excellent resolution of the Ge detectors [full width at half maximum (FWHM) of 7 keV at 7 MeV], most transitions could be individually detected. The nonresonant scattering of photons at the target, mainly responsible for the background, causes the peak-to-background ratio to worsen at lower energies, preventing the detection of weaker transitions and the determination of multipolarities. By measuring at different end point energies this problem is largely avoided. It is obvious that the background in the 6.5 MeV measurements is much lower, and hence the peak-to-background ratio improves. Therefore, and because of the feeding effects, the transitions below 6.2 MeV are deduced from the spectra taken with the 6.5 MeV beam. Between 6.2 and 6.5 MeV the photon flux from the 6.5 MeV electron beam is too low to detect weaker transitions or to extract transition strengths with high accuracy.

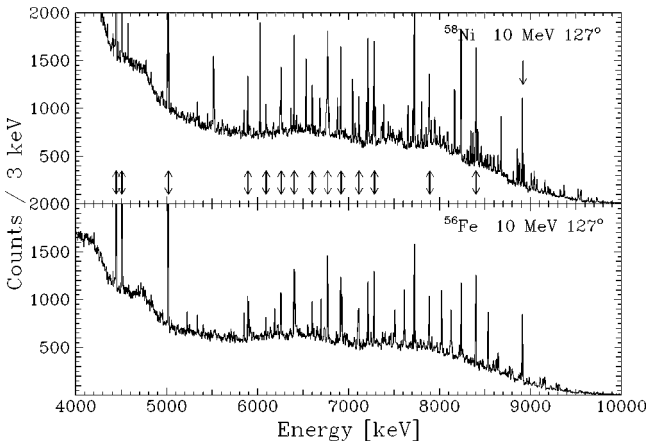

FIG. 2. Part of the ^{56}Fe and ^{58}Ni spectrum at $\theta=127°$ and $E_{\gamma,max}=10$ MeV. Arrows indicate the calibration lines (including escape lines).

Spin assignments for both nuclei are based on the angular distribution ratio (see Sec. II A) of the scattered photons. Figure 4 shows as an example the measured ratios $W(90°)/W(127°)$ for all the transitions observed between 5 and 10 MeV in the 10 MeV experiment on ^{56}Fe. The solid lines represent the expected values for dipole and quadrupole transitions. In case of an isotropic distribution (for most inelastic transitions or heavily fed ground state transitions) the ratio will be 1, as represented by the dashed line. Since the angular distribution ratios for the isotropic (1) and dipole (0.73) cases are very similar, it is dangerous to extract spin assignments for transitions where the feeding effect plays an important role (about 4 MeV below the end point energy). By considering all the angular distribution ratios below 6 MeV from the 6.5 MeV experiment only, and for the levels above 6 MeV from the 10 MeV experiment, we obtain good spin assignments for all transitions between 2 and 10 MeV.

In order to obtain parities, the measured asymmetry values from the experiments with polarized photons are com-

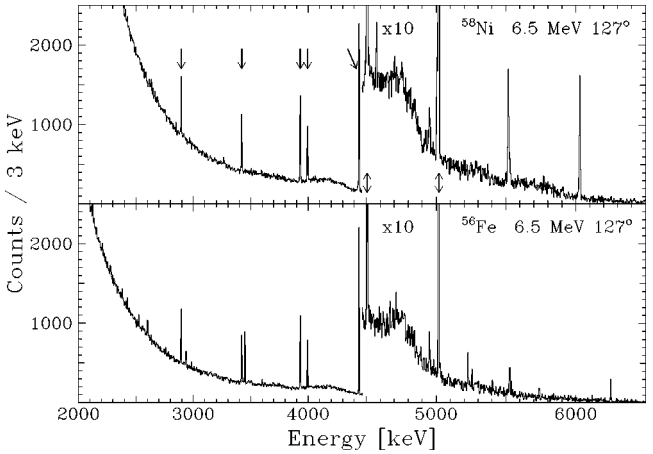

FIG. 3. Part of the ^{56}Fe and ^{58}Ni spectrum at $\theta=127°$ and $E_{\gamma,max}=6.5$ MeV. Arrows indicate the calibration lines.

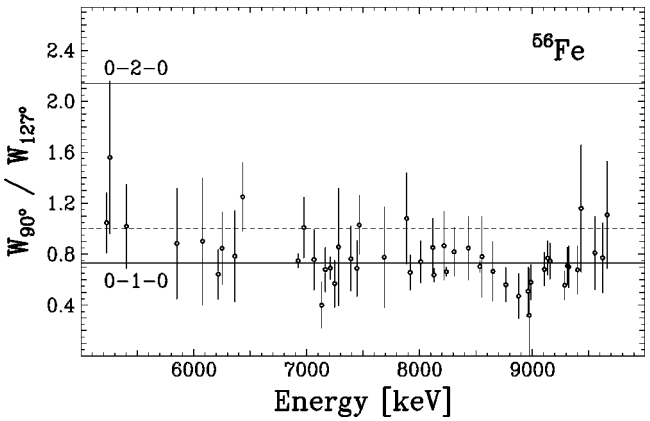

FIG. 4. Angular distribution ratio for the $E_{\gamma,max}=10$ MeV experiment on ^{56}Fe for excitation energies between 5 and 10 MeV. At lower energies feeding effects make the angular distribution isotropic $[W(90°)/W(127°)=1]$. The expected ratios for the spin sequences 0-1-0 and 0-2-0 are indicated by the solid lines. The isotropic distribution is represented by the dashed line.

pared to the polarization degree of the incident photon beam (see Sec. II A). Figure 5 displays as an example the asymmetry values for the transitions in ^{58}Ni to which a parity could be assigned. The dashed lines represent the expected bands of the asymmetry values for transitions inducing $(\pi=-)$ or not $(\pi=+)$ a parity change (the absolute asymmetry value equals the polarization degree of the beam). For transitions below 6 MeV the measured asymmetries drop quickly to zero, indicating the influence of the feeding effect.

The detection limits in the experiments with unpolarized photons are approximately the same for both ^{58}Ni and ^{56}Fe measurements, and are shown in Fig. 6. They were calculated assuming that a transition can only be observed in the spectrum if the full energy peak area is larger than 3 times the standard deviation of the underlying background. The detection limits for the ground state transition widths (Γ_0) and the $E1$ reduced transition probabilities $[B(E1)\uparrow]$ are displayed in the same graph. The 6.5 and 10 MeV measure-

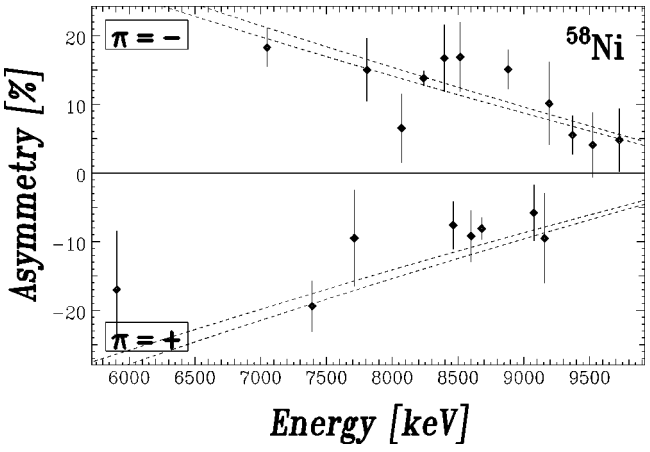

FIG. 5. The measured asymmetries for the ^{58}Ni experiment with polarized photons. Only those transitions to which a parity could be assigned are displayed. The dashed lines represent the error bands for the expected values for positive and negative parity transitions.

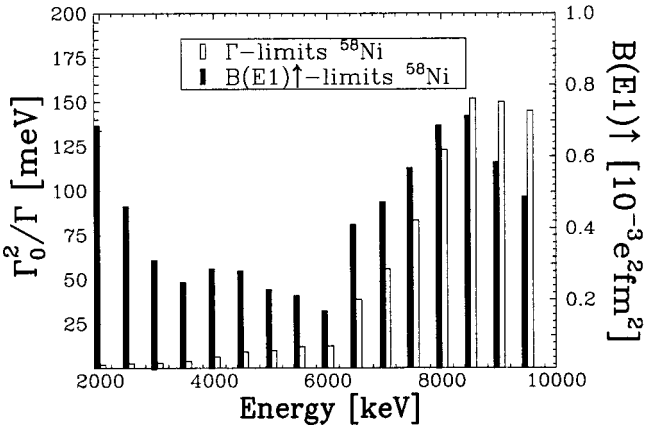

FIG. 6. The detection limits for the ground state transition width Γ_0 (left scale) and the reduced transition probability $B(E1)\uparrow$ (right scale) for the ^{58}Ni experiment. For ^{56}Fe similar limits were obtained. Up to an excitation energy of 6 MeV the 6.5 MeV spectra were used, from an excitation energy of 6.5 MeV onwards the detection limits are those from the 10 MeV experiments.

ments were combined (up to 6 MeV the 6.5 MeV spectra were used for the calculation), which accounts for the steep rise in the detection limits above 6 MeV. Over the whole energy region the $B(E1)\uparrow$ limits stay well below $10^{-3}e^2$ fm^2. The sensitivity of the experiments to polarized photons is not as good however, because the higher end point energy of 12 MeV causes the peak-to-background ratio to diminish in the energy region of our interest, notwithstanding the longer measuring times. Therefore only the parities of the strongest transitions could be determined.

A. Experiments on ^{56}Fe

Table II displays the energies, the spins, and parities, the energy integrated cross section I_s, and the transition widths Γ_0 for the 66 transitions found in ^{56}Fe. Below 6 MeV all values result from the 6.5 MeV experiment, except when indicated otherwise. In these cases, the value of I_s should be considered as an upper limit due to the expectance of quite some feeding. Spins for almost all transitions could be extracted and parities for 15 of them. The strong transition at 3448.6 keV is the well-known scissors mode [18,19], and its parity is known to be positive. The level at 3369.7 keV is described in Nuclear Data Sheets [31] as a 2^+ state, and this was adopted in our work as it is necessary to know the multipolarity for a correct calculation of the transition widths. Besides this transition, only one other quadrupole transition turned up in our experiments at 5257.1 keV. No parity could be extracted for this transition, but as $M2$ transitions are extremely weak in NRF experiments, we can assume that the parity is positive ($E2$ transition). For some transitions near the end point energy of 10 MeV no spin assignments were possible due to the poor statistics associated with the low photon flux. The transition at 5851.5 keV, only observed in the 10 MeV experiment, coincided with an inelastic transition in ^{11}B. After correction there remained a transition width Γ_0^2/Γ of 26 ± 16 meV, in good agreement with the result from Ref. [19]. All peaks corresponding to the two

TABLE II. NRF results for ground state transitions in ^{56}Fe. For states without observed branching Γ_0 was calculated under the assumption of a pure ground state transition ($\Gamma_0^2/\Gamma=\Gamma_0$). Where possible branching was observed the branching ratio is displayed and incorporated in the Γ_0 value. Parentheses indicate tentative assignments. Possible inelastic transitions are present (as indicated by footnotes), treated as ground state transitions.

Energy (keV)	J^π	I_s (eV b)	Γ_0 (meV)	Γ_0/Γ	Γ_0^2/Γ [a] (meV)	Γ_0/Γ [a]	$B(E1)\uparrow, B(M1)\uparrow$ [$(10^{-3}e^2$ fm^2), (μ_N^2)]	
9768.2±0.7		41±19	336±158		480±130			
9741.7±1.3 [b]	(1)	61±16	1618±222	0.31±0.09	950±250			
9732.2±1.6		63±19	521±152					
9664.7±0.9		53±9	429±75		670±220			
9622.9±2.5	1	59±10	473±83					
9554.8±1.3	1	86±15	680±119		390±140			
9434.9±2.3		41±9	313±71					
9402.0±0.6 [c]	1	89±12	1305±155	0.52±0.09	650±150			
9323.7±0.7	1	102±12	767±88		650±140			
9312.2±0.8	1	116±12	869±88		640±130			
9287.6±1.0	1^-	120±11	899±81		750±170		3.24±0.29	$E1$
9156.8±1.0	$1^{(-)}$	190±17	1384±122		950±310		5.20±0.46	$E1$
9137.6±0.5	1^-	117±12	844±87		570±120		3.19±0.33	$E1$
9107.8±0.8	$1^{(-)}$	116±11	838±78		860±180		3.20±0.30	$E1$
8988.9±0.6	1	91±10	639±72		310±70			
8972.2±1.1	1	25±11	173±77					
8963.6±0.7	1	65±12	454±82		380±70			
8908.9±1.2	$(1)^{(+)}$	94±46	647±316		470±100		0.238±0.116	$M1$
8879.3±0.9	1	59±10	402±68		300±80			
8766.1±0.8	1	97±12	649±78		410±80			
8652.5±0.8	1	62±11	403±70					
8554.7±0.9 [d]	1	51±10	327±65					
8536.3±0.4 [c]	1^-	395±16	2714±112	0.92±0.05	2040±310		12.52±0.52	$E1$
8343.3±0.6	1	59±9	357±52					
8307.0±0.8	1^+	74±9	445±51		240±80		0.201±0.023	$M1$
8239.6±0.5 [c]	1^-	509±12	3257±81	0.92±0.03	2630±420		16.75±0.42	$E1$
8219.4±0.6	1	64±10	372±58		260±50			
8128.7±0.4	1^-	266±11	1526±61		1940±300		8.19±0.33	$E1$
8119.6±0.8	1	68±9	391±52					
8011.9±0.6 [c]	1	73±8	547±48	0.75±0.10				
7917.9±0.4	1^+	70±7	380±39				0.199±0.020	$M1$
7887.6±0.7	(1)	73±17	396±92		280±50			
7763.6±0.6	(1)	33±13	170±69					
7689.8±0.6 [d]	1	25±6	128±32					
7467.6±0.5	1^+	54±11	260±55		180±30		0.162±0.034	$M1$
7446.2±0.6	1	39±6	189±30		170±50			
7392.5±0.4 [d]	1	34±6	161±27					
7282.2±0.7	1	58±9	266±41		290±120			
7249.4±0.5	1^+	48±7	219±34		200±30		0.149±0.023	$M1$
7211.1±0.3 [e]	1^+	112±7	614±38	0.82±0.05	500±80		0.425±0.026	$M1$
7166.0±0.7 [f]	1^-	39±5	175±22		89±15		1.37±0.17	$E1$
7134.6±0.7	1	29±7	130±31		56±10			
7066.4±0.9 [c,g]	1	32±5	268±28	0.51±0.10	110±20	0.63±0.04		
6977.4±0.5 [d]	1	36±6	153±25					
6925.4±0.3 [c]	1^-	162±5	750±31	0.90±0.05	700±110	0.92±0.01	6.52±0.27	$E1$
6433.7±0.6 [d]	1	37±10	134±35					
6365.0±0.6	1	22±5	76±17					

TABLE II. (*Continued*).

Energy (keV)	J^π	I_s (eV b)	Γ_0 (meV)	Γ_0/Γ	Γ_0^2/Γ [a] (meV)	Γ_0/Γ [a]	$B(E1)\uparrow, B(M1)\uparrow$ $[(10^{-3}e^2\ \mathrm{fm}^2), (\mu_N^2)]$
6251.2±0.6 [c]	1	25±4	166±19	0.52±0.09	56±13	0.54±0.04	
6218.2±0.6 [d,h]	1	25±3	82±11		34±8		
6078.4±1.5 [d,h]	(1)	15±4	48±13		28±5		
5851.5±0.4 [h]		8.9±5.4	26±16		24±6		
5571.4±1.1	(2)	3.4±1.3	9.2±4.9				
5538.4±0.8	1	7.3±1.6	20±4				
5403.6±0.8 [d]	1	9.3±2.4	24±6		27±6		
5257.1±0.5 [c]	2	14±2	30±6	0.67±0.10	23±4		
5227.8±0.4	1	18±3	42±6		37±6		
4846.1±0.8 [h]		7.7±2.3	16±5		7.1±3		
4669.4±0.5	(1)	6.2±2.0	12±5				
4409.7±0.4 [d]	(2)	3.6±1.1	6.0±2.6				
3605.5±0.4 [f]	(1)	9.6±2.6	11±4		11±2		
3448.6±0.2 [c]	1^+	60±3	78±5	0.79±0.06	77±12	0.79±0.02	0.494±0.032 $M1$
3369.7±0.5 [c,h]	2^+	14±3	47±6	0.17±0.05			
2983.1±0.4	1	6.0±1.4	4.6±1.6				
2763.5±0.4 [h]		14±2	9.4±1.1				
2742.7±0.9		2.9±1.0	1.9±0.9				
2133.1±0.2 [h]		41±3	16±1				
						$\Sigma B(E1)\uparrow$	60.2±1.1
						$\Sigma B(M1)\uparrow$	1.87±0.14

[a]From Ref. [19].
[b]Possible branching observed to the 2763.5 keV level.
[c]Possible branching observed to the first 2^+ level at 847 keV.
[d]Possibly inelastic transition.
[e]Possible branching observed to the 3605.5 keV level.
[f]Possibly partly inelastic.
[g]The branching to the 847 (2^+) keV level was indicated in Ref. [19]. In this work the Ritz rule had to be applied with two standard deviations instead of one to reach the same conclusion.
[h]Observed only in 10 MeV measurement; strengths include feeding effects.

transitions at 7887.6 and 7763.6 keV were contaminated by calibration or other ^{56}Fe lines in the spectrum and their strengths should be treated with some caution, although the relatively large errors reflect the necessary corrections for the contamination.

In the sixth column of Table II, a comparison is made with the Γ_0^2/Γ values from the NRF experiments by Chapuran *et al.* [19] with electron beams of 10.3 and 7.6 MeV. Besides the detection of 24 new transitions and the determination of 41 unknown multipolarities, two previously observed doublets could be resolved in our work. The doublet at 9737±5 keV [19] was resolved into two lines at 9741.7 and 9732.3 keV. The transition width of the doublet is in good agreement with the summed value of both transitions. The doublet at 3602±3 keV [19] was resolved into two transitions at 3605.5 and 3600.3 keV. The latter is not included in Table II since it is an inelastic transition, as stated in Nuclear Data Sheets [31]. In Ref. [19] the transitions at 9107.8, 8963.6, and 8128.7 keV were considered as multiplets, but no indication for this was found in our experiments. A transition at 7917.9 keV is also included in Table II. According to Chapuran *et al.* [19], this transition comes from the copper used in the shielding [^{nat}Cu(n,γ), $E_\gamma = 7916\pm1$ keV [32]]. It must be a ^{56}Fe transition however, because of the following reasons: Almost no copper was used in the shielding of our setup. The transition is also not visible in other spectra (^{58}Ni, H_3BO_3). Two other strong ^{nat}Cu(n,γ) lines at 7637 and 7307 keV should be visible alongside, but they are not. Furthermore, the transition in question exhibits a distinct angular distribution (dipole) and azimuthal asymmetry ($-18\pm9\%$), indicating an $M1$ character. Considering all these arguments, one can conclude that the transition at 7917.9 keV must belong to ^{56}Fe.

There were no contradictions in spin assignments between both experiments and the calculated ground state transition width ratios Γ_0^2/Γ agree in general within the error. Between 6 and 7.6 MeV (the lowest bremsstrahlung end point energy used in Ref. [19]) there could be deviations due to feeding effects connected with the high end point energy of 10 MeV in our measurements. This is the case for the first three transitions above 6 MeV. For two levels at 7166.0 and 7134.6 keV there is also a discrepancy, although we expect the feeding effects to be minimal in this energy region. It is worth

noticing, however, that the strengths measured by Chapuran *et al.* [19], only for these two close-lying transitions, lie below the detection limits (100 meV at 7 MeV) of their experiment. Therefore we consider our results more reliable. The good agreement elsewhere shows again, as stated in Ref. [19], that the strengths obtained for five levels in the photon scattering experiments by Kumagai *et al.* [17] are systematically too high. Also the Γ_0^2/Γ value of 1280 ± 170 meV for the 9137.6 keV transition obtained in an NRF experiment with monoenergetic γ rays [33] seems rather much overestimated.

In a recent NRF measurement with a 6.6 MeV electron beam on ^{56}Fe by Ishkanov *et al.* [18] the energies and transition widths of eight transitions were detected between 3 and 6.6 MeV. For most transitions there is no contradiction with our work. The $M1$ scissors mode at 3448.6 keV seems somewhat weaker in our measurement however. Since the resolution in Ref. [18] was quite worse (FWHM of 8 keV at 2 MeV), the doublet around 3602 keV was not resolved and treated as one 2^+ transition, hence the discrepancy in strengths with this work. The two transitions at 6251.2 and 4846.1 keV are probably overestimated in our measurement, but because they were taken from the 10 MeV experiment, feeding effects can account for this.

The parities extracted from the $^{56}\mathrm{Fe}(\vec{\gamma},\gamma)$ experiment largely confirm the results from the earlier NRF experiments performed in Giessen [9] and the test measurement in Gent [20] with two exceptions. In both Gent experiments, the 7211.1 keV transition clearly posesses a positive parity, instead of the negative parity deduced in Giessen. For the transition at 9107.8 keV, our experiment yields a tentative negative parity, in contrast to both earlier experiments. Obviously, despite the higher statistics in this work, the statistical nature of these experiments produces contradictory results in this case.

It is inevitable that some of the transitions in Table II are the result of a decay to an intermediate level and not to the ground state. This has not only consequences for the observed transition in question (the observed cross section is connected to $\Gamma_0\Gamma_i/\Gamma$, with Γ_0, Γ_i, and Γ the transition widths of the decaying level to the ground state, the intermediate state, and the total decay width, respectively), but also for the decaying level whose Γ_0 value will become larger than the observed Γ_0^2/Γ. These inelastic transitions were searched for by applying the Ritz rule to the energies and their uncertainties of all observed transitions, completed with known energies of low-lying levels [31]. The resulting transitions are indicated in Table II by means of footnotes. The levels from which these transitions evolve are indicated in the same way. The branching ratios to the ground state (Γ_0/Γ) for these levels are also displayed. To calculate these branching ratios, only the observed branching to intermediate states was taken into account. Because of possible not observed branching to other intermediate levels, the calculated ground state transition widths Γ_0 should be considered as a lower limit. As can be seen, most of the indicated levels possibly branch to the first excited 2^+ state at 847 keV, which is energetically most favored.

One must keep in mind that the Ritz rule only indicates a possibility for decay to the intermediate state. Therefore the resulting inelastic transitions are still present in Table II and treated as ground state transitions. The two lowest inelastic transitions at 2523.0 [$3369.7 \rightarrow 847\ (2^+)$] and 2601.6 [$3448.6 \rightarrow 847\ (2^+)$] keV are not included, however, since their inelastic nature was determined in other experiments and adopted as such in Nuclear Data Sheets [31]. The Ritz rule established some more candidates for inelastic γ cascades, but those could be ruled out on the basis of a comparison between the experiments at different end point energies (10, 7.3, 6.6, and 6.5 MeV) and by comparing expected cross sections with the sensitivity limits of the different measurements.

For all levels below 6.5 MeV, except the 3369.7 keV level, the branching ratio could be extracted from the 6.5 MeV as well as the 10 MeV measurement. No contradictions were found, which stresses the high probability of these branchings. For these, the weighted average of both branching ratios was calculated, and displayed in Table II.

The transitions at 7166.0 and 3605.5 keV can only be partially inelastic, because they were also observed in the experiments with lower end point energy. By correcting the 10 MeV strengths with the ones found in the 6.5 and 7.6 MeV experiments, the (possibly) inelastic parts and the resulting branching ratios could be calculated.

In column 7 of Table II a comparison for the branching ratios is made with the results from Ref. [19]. Within the error bars there is agreement in all cases, and especially for the $M1$ scissors mode at 3448.6 keV. It is also worth mentioning that the branching ratio for this level extracted from the 10 MeV experiment (0.79 ± 0.09) equals the one from the 6.5 MeV experiment (0.79 ± 0.07). The branching ratio from the experiments by Ishkanov *et al.* [34] also lies within the error (0.77 ± 0.02). In a recent self-absorption experiment [34], the half-life of the scissors mode at 3448.6 keV was determined to be 3.65 ± 0.32 fs [34]. The value from the present work, with the observed branching included, amounts to 5.85 ± 0.37 fs. The discrepancy may perhaps be due to some small unobserved branchings of this level (the final Γ_0/Γ should then amount to 0.50 ± 0.7).

Two other branching possibilities are mentioned in Ref. [19]: the level at 9154 keV [$9154 \rightarrow 847(2^+)$ keV $= 8307$ keV] and the one at 6698 keV [$6698 \rightarrow 847(2^+)$ keV $= 5853$ keV]. For the first level the Ritz rule did not indicate a branching possibility, even when using two standard deviations. In the second case the branching level at 6698 keV itself was not observed in our spectra. However, Ishkhanov *et al.* [18] observed the 5853 keV transition using a 6.6 MeV electron beam, and obtained a strength similar to that obtained in our 10 MeV experiment, ruling out an inelastic origin.

The final ground state transition widths from Table II were used to calculate the reduced transition probabilities for the identified $E1$ and $M1$ transitions [$B(E1)\uparrow$, $B(M1)\uparrow$]. These are displayed in the last column of Table II. The strengths of the individual transitions were added to obtain the total identified $E1$ and $M1$ strength, which is shown at the bottom of the table. This total strength should of course

be considered as a lower limit because the parity of a large number of weak transitions remains unknown. The strongest transitions were identified as $E1$ or $M1$ however, so the total strength is not expected to increase more than about a factor of 2.

B. Experiments on ^{58}Ni

Table III displays the 64 observed transitions in ^{58}Ni. As in the previous section, all transitions below 6 MeV are from the 6.5 MeV experiment, except indicated otherwise. Spins for most transitions above 6 MeV could be determined except in two cases. For the transition at 8068.6 keV we can assume a dipole character however, because the parity turned out to be negative (see Fig. 5). Since $M2$ transitions are very unlikely to be observed in a photon scattering experiment, a tentative dipole character can be assigned to this transition. Several quadrupole transitions were also detected, mainly below 4 MeV. For the same reason as mentioned above, a positive parity can be assumed for these. Above 4 MeV only one tentative quadrupole transition was observed at 7595.9 keV. Many of the transitions below 6 MeV were observed only in the 10 MeV experiment, indicating considerable feeding or an inelastic origin at these energies. Consequently the angular distribution shows a more isotropic behavior, preventing spin assignments.

Column 6 of Table III displays the results from the earlier NRF experiment by Ackermann *et al.* [21]. They observed ten transitions, of which nine were also detected in this work. The remaining one, at 9843 ± 5 keV, is too high in energy to be detected due to the low photon flux near the end point energy. There were no contradictions in spin assignments, and most values for Γ_0 and Γ_0^2/Γ agree within the error bars. Nevertheless, the transitions at 9667.8 and 8679.3 keV seem to disagree substantially from Ref. [21], notwithstanding their large uncertainties in that measurement.

The experiment with polarized bremsstrahlung yielded 11 negative parities (of which three tentative) and eight positive ones (of which one tentative). These are all connected with transitions with multipolarity 1, and hence are $E1$ or $M1$ transitions. The quadrupole transitions in the table can be assumed to have positive parity. In an unpublished measurement performed in Giessen [22] with polarized bremsstrahlung the parities for four transitions have been determined. There were no contradictions with this work. For two transitions the tentative character of the parity could be made certain. The tentative negative parity for the 6027.3 keV transition could not be confirmed however.

Compared to the results for ^{56}Fe, it is remarkable how many transitions below 4 MeV are observed in ^{58}Ni, practically all observed in the 10 MeV spectra only (especially prominent are the strong transitions at 2598.4 and 3253.7 keV). A high degree of feeding could be the cause, but as the level scheme of this low-energy region is considered quite well known, it is not very probable. Perhaps most of these transitions are inelastic ones. The results from the search for possible inelastic transitions, using the Ritz rule, are displayed separately in Table IV. The energies of the decaying level, E_x, of the final level, E_f, and of the intermediate inelastic transition, E_i, are displayed, as well as the resulting branching ratio Γ_0/Γ and the final ground state transition width Γ_0. In contrast to the results for ^{56}Fe, only about one-third of the observed branching occurs to the first 2^+ state at 1454 keV. The possible inelastic transitions are again also present in Table III as ground state transitions. Only the two lowest transitions are not included (2140.6 and 1809.8 keV) because the related $3595.2 \rightarrow 1454$ and $3263.9 \rightarrow 1454$ keV cascades were already adopted in Nuclear Data Sheets [35]. The Ritz rule yielded some more branching possibilities, but these could be ruled out by comparing the results at different end point energies, by comparing with the Nuclear Data Sheets level scheme [35] or in the case of the $9523.3 \rightarrow 1454$ keV cascade by considering the known parities of the three involved transitions.

The level at 9630.5 keV can, according to the Ritz rule, branch in three different ways. Since some of these can be coincidental, the three possibilities are shown in Table IV with their respective branching ratios and final Γ_0 values. In fact, each combination of these branchings is possible. The branching to a 2034.6 keV level is considered less likely: The related 2034.6 keV and the 7595.9 keV transitions have been observed as $E2$ transitions. Hence the 9630.6 keV transition should also have a positive parity. Although no definite parity for this transition could be determined, a positive value is quite unlikely: The measured asymmetry was $(14 \pm 7)\%$, while the expected value for a positive parity is -5.6%, thus pointing more in the direction of a negative parity. Therefore we adopted in Table III the combination of the two remaining possibilities, and the resulting branching ratio then amounts to 0.38 ± 0.06. For the three branching possibilities together the branching ratio would be 0.25 ± 0.03 and the final ground state transition width Γ_0, 1815 ± 150 meV.

For the 8395.1 keV level two branching possibilities have been found. They are also separately displayed in Table IV with their respective branching ratios. For the final branching ratio, as displayed in Table III, the two possibilities were combined, yielding a total branching ratio of 0.71 ± 0.11.

It is also noticeable from Table IV that the 6424.9 keV transition can be an inelastic line originating from two different levels. Since there is no indication of a doublet structure for this transition, it most probably belongs to only one of the two branchings. As no further indication of its origin can be found, the two branching ratios are both present in Table III.

The last column of Table III lists the identified $E1$ and $M1$ transitions, with their respective $B(E1)\uparrow$ and $B(M1)\uparrow$ reduced transition probabilities. The total detected $E1$ and $M1$ strengths are displayed at the bottom. As in the ^{56}Fe case, these should be considered as a lower limit as the parity of many weaker transitions is unknown.

IV. DISCUSSION AND COMPARISON

A. $E1$ strength

It is clear from the previous section that for both ^{58}Ni and ^{56}Fe, the strongest transitions by far turned out to be of $E1$

TABLE III. The same as Table II but for ^{58}Ni.

Energy (keV)	J^π	I_s (eV b)	Γ_0 (meV)	Γ_0/Γ	Γ_0^2/Γ [a] (meV)	$B(E1)\uparrow, B(M1)\uparrow$ $[(10^{-3}e^2\ \mathrm{fm}^2),\ (\mu_N^2)]$	
9723.0±0.9	$1^{(-)}$	90±8	1760±128	0.42±0.05		5.52±0.40	*E*1
9667.8±1.5	1	68±12	812±166	0.67±0.18	1910±690		
9630.5±2.4	1	57±6	1189±116	0.38±0.06[e]			
9554.0±2.1	1	172±11	1362±84		1530±610		
9523.3±1.3	1^-	165±10	2250±146	0.58±0.05		7.51±0.49	*E*1
9455.4±1.8	1	29±5	222±42				
9368.5±0.6	$1^{(-)}$	163±15	1238±115		1260±480	4.34±0.40	*E*1
9326.4±0.8	1	93±6	975±63	0.72±0.07[f]			
9190.7±0.5	1^-	108±10	791±75		1010±400	2.94±0.28	*E*1
9156.9±0.7	1^+	82±11	594±79			0.201±0.027	*M*1
9073.4±0.6	$1^{(+)}$	124±9	888±60			0.309±0.021	*M*1
8961.3±0.7	1	54±6	378±39				
8934.6±0.5	1	213±8	1474±52				
8880.2±0.6	1^-	171±7	1170±45			4.81±0.18	*E*1
8857.4±0.6	1	110±22	751±147				
8679.3±0.8	1^+	314±16	2052±103		1160±400	0.815±0.041	*M*1
8600.5±0.7	1^+	125±12	803±80			0.328±0.033	*M*1
8552.7±1.3	(1)	74±7	470±44				
8514.1±0.4	1^-	109±8	686±51			3.20±0.24	*E*1
8461.0±0.7	1^+	144±8	893±48			0.383±0.021	*M*1
8395.1±1.2	1^-	101±12	836±78	0.74±0.11		4.07±0.38	*E*1
8317.1±1.7	1	40±6	239±36				
8237.3±0.4	1^-	610±9	3590±55		2960±460	18.51±0.28	*E*1
8096.3±0.6	1	50±9	284±52				
8068.6±1.2[b,c]	$(1)^{(-)}$	59±8	331±43			1.81±0.23	*E*1
7876.7±2.6	1	44±13	340±72	0.69±0.25[f]			
7807.3±0.5	1^-	107±13	564±67			3.42±0.41	*E*1
7766.0±0.7	(1)	23±4	122±20				
7709.7±0.6	1^+	123±5	632±23		490±200	0.358±0.013	*M*1
7616.0±1.0[c]	(1)	9.5±4.1	48±20				
7595.9±0.6[c]	(2)	29±5	88±13				
7585.1±0.6		18±8	89±41				
7388.8±0.4	1^+	97±5	457±24			0.294±0.016	*M*1
7271.7±0.7	1	100±10	456±45				
7249.6±1.1	(1)	11±4	49±17				
7048.2±0.9	1^-	128±4	552±17		690±260	4.55±0.14	*E*1
6892.9±1.5[c]	(1)	9.7±4.9	40±20				
6685.0±0.9[c]	1	33±4	126±14				
6430.7±1.0[c]	1	18±2	66±7				
6424.9±0.9[c]	1	14±2	49±7				
6027.3±0.7	1	112±3	435±12	0.81±0.03	330±110		
5905.3±0.7	1^+	10±2	18±3			0.023±0.004	*M*1
5528.0±0.4[d]	(1)	21±3	56±8				
5452.2±0.4[c,d]	1	12±2	30±4				
5394.0±0.9		4.2±1.0	11±2				
5359.3±1.6[c,d]		4.8±1.2	12±3				
4954.0±0.8	1	15±2	32±5				
4574.1±0.5[c]	1	12±2	22±3				
4106.4±1.0[d]		18±2	27±2				
3943.6±1.2[d]		12±3	16±3				
3595.2±0.9		6.9±1.4	33±8	0.24±0.03			

TABLE III. (*Continued*).

Energy (keV)	J^π	I_s (eV b)	Γ_0 (meV)	Γ_0/Γ	Γ_0^2/Γ [a] (meV)	$B(E1)\uparrow, B(M1)\uparrow$ $[(10^{-3}e^2\ \mathrm{fm}^2), (\mu_N^2)]$
3450.9±0.5 [d]		36±4	37±4			
3273.7±0.7 [d]	(2)	14±2	7.8±1.1			
3269.1±0.8 [d]	(2)	12±2	6.7±1.1			
3263.9±0.6	2	10±1	12±3	0.47±0.1		
3253.7±0.4 [d]		82±4	75±4			
3202.2±0.3 [d]		30±4	27±4			
3037.8±0.7	2	3.2±0.8	1.5±0.4			
2741.8±0.7 [d]	(2)	12±3	4.6±1.0			
2632.8±1.3	(1)	6.7±1.8	4.0±1.1			
2598.4±0.3 [d]		134±15	78±9			
2385.1±0.9	(2)	5.9±1.3	1.7±0.4			
2034.6±0.3 [d]	2	67±5	14±1			
2014.9±0.4 [d]		23±3	7.9±1.1			
					$\Sigma B(E1)\uparrow$	60.7±1.1
					$\Sigma B(M1)\uparrow$	2.71±0.07

[a]From Ref. [21].
[b]No spin assignment was possible. Since $M2$ (2^-) transitions are very unlikely to occur, we chose for a tentative $E1$ assignment.
[c]Possibly inelastic transition.
[d]Observed only in 10 MeV measurement; strengths include feeding effects.
[e]Branching ratio calculated for branching to 2014.9 and 3202.2 keV levels. See text.
[f]The involved inelastic transition at 6424.9 keV can belong to two different branching scenarios. Probably only one is genuine.

character. Of course, one expects quite some $E1$ strength in this region due to the tail of the GDR, which extends into the bound region, but our experiments reveal a concentration in one (^{58}Ni) and three (^{56}Fe) strong transitions situated around 8.2 MeV. These transitions alone represent 1/3 (^{58}Ni) or 1/2 (^{56}Fe) of the total identified $E1$ strength. Figures 7(a) and 8(a) show the observed $E1$ transitions and their reduced transition probabilities $B(E1)\uparrow$ for both nuclei (bars). These results have also been smeared out with a Breit-Wigner function with a width of 0.3 MeV to obtain a strength function $b(E1,E)\uparrow$ (curve) that incorporates the clustering of transitions near each other. The total identified $E1$ strength, which is comprised in both cases between 5.9 and 10 MeV, is very similar in both nuclei: 60.2±1.1 and 60.7±1.1 $\times 10^{-3}e^2$ fm^2, respectively, in ^{56}Fe and ^{58}Ni.

TABLE IV. Possible branching in ^{58}Ni. See text for complete discussion.

E_x (keV)	E_f (keV)	E_i (keV)	Γ_0/Γ	Γ_0 (meV)
9723.0±0.9	3037.6±0.7	6685.0±0.9	0.42±0.05	1760±128
9667.8±1.5	2775.5±0.2 [a]	6892.9±1.5	0.67±0.18	812±166
9630.5±2.4	2014.9±0.4	7616.0±1.0	0.69±0.13	658±100
	(2034.6±0.3)	(7595.9±0.6)	(0.42±0.06)	(1083±108)
	3202.2±0.3	6430.7±1.0	0.46±0.06	987±77
9523.3±1.3	1454 (2^+)	8068.6±1.2	0.58±0.05	2250±146
9326.4±0.8	2901.8±0.2 [a]	6424.9±0.9 [b]	0.72±0.07	975±63
8395.1±1.2	2942.4±0.2 [a]	5452.2±0.4	0.80±0.12	771±76
	3037.6±0.7	5359.3±1.6	0.90±0.15	680±75
7876.7±2.6	1454 (2^+)	6424.9±0.9 [b]	0.69±0.25	340±72
6027.3±0.7	1454 (2^+)	4574.1±0.5	0.81±0.03	435±12
3595.2±0.9	1454 (2^+)	2140.6±0.1	0.24±0.03	33±8
3263.9±0.6	1454 (2^+)	1809.8±1.1 [c]	0.47±0.01	12±2

[a]Level not observed in this work, but adopted from Nuclear Data Sheets [35].
[b]This inelastic transition can be connected with two different branching scenarios; probably only one is genuine (see text).
[c]This transition was observed in the 6.5 MeV measurement.

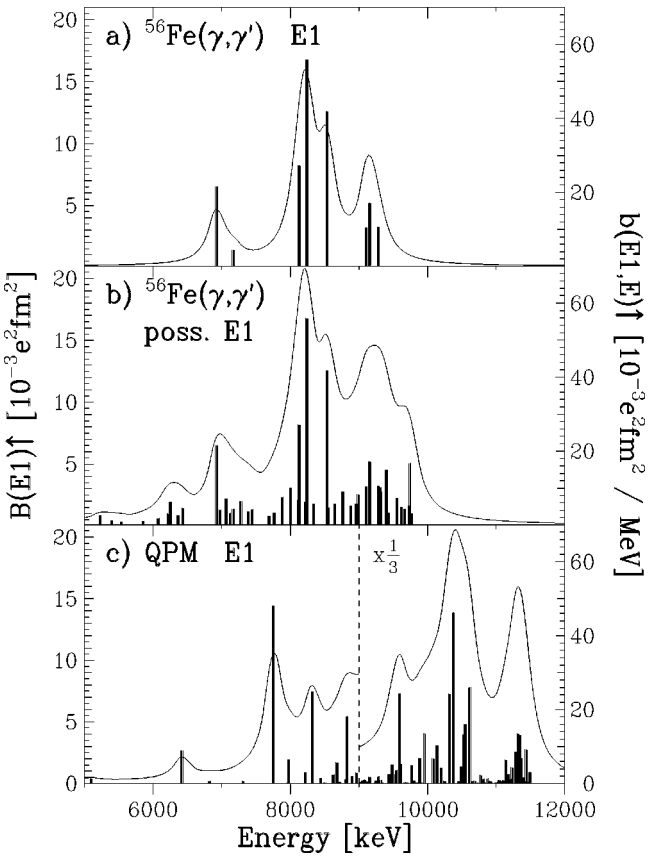

FIG. 7. $E1$ strength in ^{56}Fe from 2 to 12 MeV. Bars represent the individual transitions (left-hand scale). The curve (right-hand scale) represents the same results, but smeared out with a Breit-Wigner function with smearing parameter of 0.3 MeV. Part (a) displays transitions with an $E1$ assignment. In part (b) all observed transitions are included (including possible inelastic transitions), except those who could be identified as $M1$ or quadrupole. Part (c) displays the results of the QPM calculations.

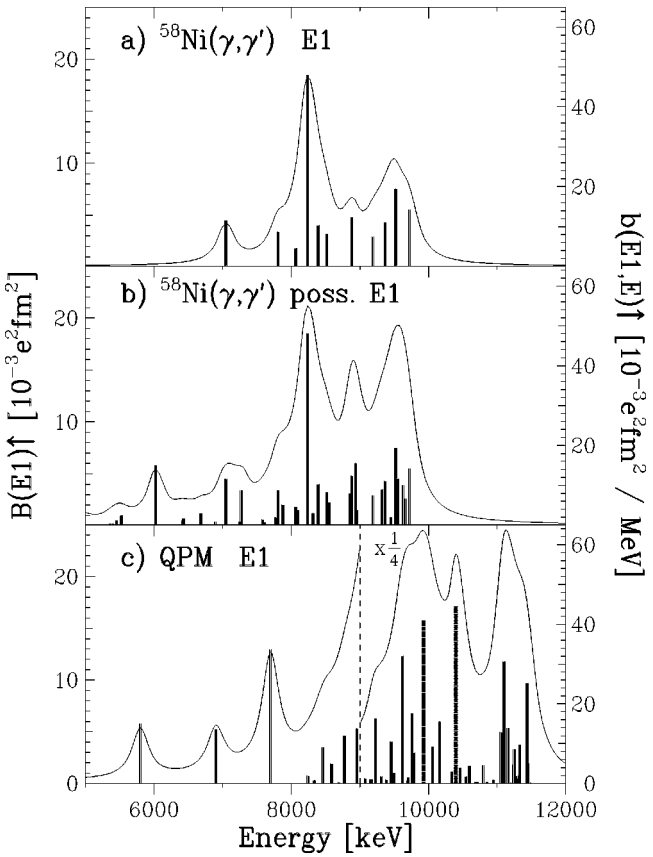

FIG. 8. The same as Fig. 7 but for ^{58}Ni.

In Figs. 7(b) and 8(b) all the possible $E1$ transitions are displayed (meaning all $E1$ transitions and those who could not be identified as $M1$ or $E2$ transitions, including inelastic transitions) together with the smeared-out curve. Below 5 MeV we expect little $E1$ strength and therefore most of these transitions are probably of $E2$ character or unidentified inelastic transitions (certainly in the case of ^{58}Ni, as discussed in the previous section). To be consistent with an increase of $E1$ strength towards higher energies (in agreement with the shape of the Lorentz tail of the GDR), most of the transitions at these higher energies (and certainly above 9 MeV) should be considered as $E1$ transitions, as can be seen clearly from the smeared-out curve. However, the strongest transitions in both nuclei still seem to impose an additional $E1$ resonance around 8.2 MeV upon this tail. This resonance has a comparable strength in both nuclei but is somewhat broader in ^{56}Fe due to the fragmentation over three strong transitions. The total resulting strength between 5 and 10 MeV, when including all transitions shown in Figs. 7(b) and 8(b), amounts then to 127 ± 2 (^{56}Fe) and 109 ± 2 (^{58}Ni)$\times10^{-3}e^2$ fm^2, which must be regarded as upper limits.

In an attempt to estimate the strength missing in our experiments due to the concealment of weak transitions in the background, we can compare our results for ^{56}Fe with the tagged photon experiment of Ref. [19]. In these experiments the use of tagged photons compensates a loss of resolution with the absence of any noticeable background. The binning of the results in bins of 50 to 150 keV and the absence of background also allow the strengths from weak transitions to be present in the spectra. The elastic and inelastic (leaving ^{56}Fe in its first excited state at 847 keV) cross sections were measured for excitation energies from 6 to 11.2 MeV. A direct comparison between our (γ,γ') results and the tagged photon ones is shown in Fig. 9. The solid line represents the total elastic cross section $\sigma_{\gamma\gamma}$ (based on Ref. [19]), displayed as histogram to reflect the used binning widths. The energy integrated cross sections I_s from this report are shown as bars (right scale). One can immediately notice the correspondence between structures in the tagged photon cross section and individual transitions. Only above 8.6 MeV does the cross section seem composed of many weaker transitions. To obtain a more quantitative comparison, the NRF results are smeared out with a Breit-Wigner function of variable width (in accordance with the binning width used in Ref. [19], ranging from 50 to 150 keV) and plotted as a dotted curve. The overall agreement is quite good. The overshoot for the three strong transitions is due to the fact that, in the tagged photon experiment, no self-absorption corrections were included, diminishing the observed cross section specifically for strong transitions. Even at higher energies little strength

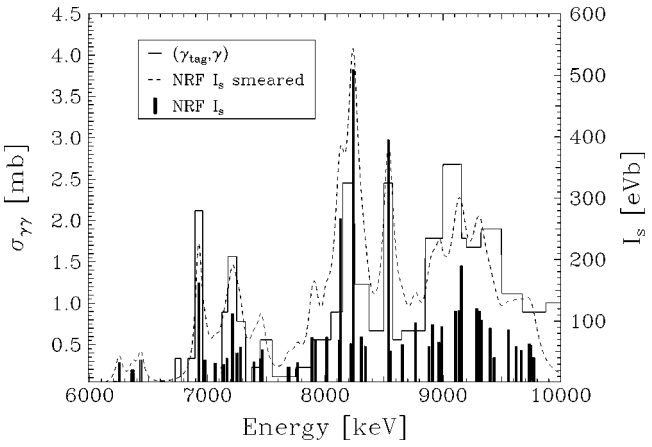

FIG. 9. Comparison between the tagged photon cross section from Ref. [19] (solid line) and the energy integrated cross sections I_s from the NRF experiments (bars, right-hand scale). The latter results were smeared out with variable width to obtain the cross section with similar resolution as for the tagged photon cross section (dotted line).

seems to be missed in our NRF measurements. It is also worth noticing that the cross section between 9.3 and 10 MeV is indeed decreasing with energy (rising again at 10.5 MeV), and is not due to the low photon flux near the end point energy in our experiments. We can thus assume that the missing strength for ^{56}Fe is not quite large. Since one can expect the fragmentation of strength in ^{58}Ni to be even less than in ^{56}Fe, due to its semimagic nature, it is safe to draw the same conclusion also for ^{58}Ni. As only part of this missing strength will be carried by $E1$ transitions, the above-mentioned upper limits for the $E1$ strength will be rather accurate.

To provide a theoretical basis for the observed transitions, microscopic calculations for excitations up to 12 MeV were performed in the framework of the QPM. These calculations, described in detail in Ref. [1], include complex configurations up to the coupling of three phonons. Since the one-phonon configurations were truncated at an energy of 25 MeV, the influence of the GDR on the 1^- states was fully taken into account, and no renormalization of effective charges in the $E1$ operator had to be carried out. This method has proved to be very accurate in describing the $E1$ response near the particle threshold in spherical nuclei [1,3] and, lately, also for describing the fragmentation of strength at lower energies [36] and in odd nuclei [37]. In general, a destructive interference between the one- and two-phonon components was observed at low energies (the $|2_1^+ \otimes 3_1^-;1^-\rangle$ state) while at higher energies the opposite effect is taking place, leading to an enhanced $E1$ strength (around 6 MeV for ^{116,124}Sn [1] and ^{140}Ce [3]). The interplay with the three-phonon configurations mainly leads to further fragmentation and redistribution of strength.

The results for ^{56}Fe and ^{58}Ni are displayed in Figs. 7(c) and 8(c) (bars). The strength function $b(E1,E)\uparrow$ (curve) has the same smearing parameter (0.3 MeV) as that for the experimental results. The whole bound region, which is accessible through NRF, is thus covered in the QPM calculations: up to 11.2 MeV for ^{56}Fe and 12.2 MeV for ^{58}Ni. Both nuclei were considered spherical, which is an accurate description for the semimagic ^{58}Ni, whereas ^{56}Fe is probably somewhat deformed [38–40] ($\delta=0.17$–0.20 [18], $\beta=0.16$ [38]).

At first sight there is no one-to-one correspondence between experiment and calculation, but this is surely beyond the scope of the QPM, certainly at higher energies where the fragmentation becomes quite important. In general, the calculations show more $E1$ strength and less fragmentation in ^{58}Ni due to the semimagic nature of this nucleus. Below 5 MeV, approximately the expected energy of the first 1^- state with a two-phonon character ($|2_1^+ \otimes 3_1^-;1^-\rangle$), no other 1^- states appear. So most unidentified, experimentally observed, transitions below this energy can indeed be considered as $(2^+ \rightarrow 0_{gs}^+)E2$ or inelastic transitions. Therefore it is more meaningful to compare strengths between 5 and 10 MeV only. For ^{56}Fe, the upper limit for the $E1$ strength in this energy region amounts to $127\times10^{-3}e^2$ fm^2, which is in very good agreement with the calculated value of $110\times10^{-3}e^2$ fm^2. In ^{58}Ni, the experimental maximum value of $110\times10^{-3}e^2$ fm^2 lies somewhat lower than calculated ($250\times10^{-3}e^2$ fm^2), but this is mainly due to the appearance of the strong resonance above 9 MeV. A slight shift or redistribution of the calculated transitions can alter this value to great effect.

For the discrepancy in strength above 9 MeV two reasons can be brought forward: (i) At higher energies the calculations will definitely underestimate the fragmentation of the strength because of the necessary truncation of the basis. Individual transitions, which fall below the detection limits of the measurements, will not be observed and hence will not contribute to the experimental strength. (ii) Since the number of appropriate intermediate states, to which branching can occur, increases greatly at higher energies, the possibility of decay into these states, including cascades, increases with it. As the observable (γ,γ') cross section in NRF is connected to Γ_0^2/Γ, any of these cascade decays will ''drain'' the cross section, possibly even below the detection limits. In cases where the branching is not so large but is not fully observed, the branching ratio Γ_0/Γ cannot be calculated completely and the resulting $E1$ strength will be underestimated.

The calculations for ^{58}Ni produce the 1^- two-phonon state ($|2_1^+ \otimes 3_1^-;1^-\rangle$) at an energy of 5800 keV with a strength $B(E1)\uparrow=6\times10^{-3}e^2$ fm^2. The energy is very close to the sum of the first 2^+ (1454 keV) and the first 3^- (4475 keV) state, which is 5929 keV. None of the identified $E1$ transitions in ^{58}Ni can be connected with this two-phonon state. There is, however, a dipole transition at 6027 keV for which no parity could be extracted, which has a comparable strength of $5.8\pm0.2\times10^{-3}e^2$ fm^2, when considered as an $E1$ transition. Its energy is about 100 keV above the sum of the constituent phonons. In the heavier $Z=50$ isotopes and $N=82$ isotones, however, this two-phonon state lies about 200 keV below the sum [41–43]. To confirm its two-phonon nature, one should compare its decay into the 2^+ or the 3^- phonon to the transitions strengths of, respectively, the 3^- or 2^+ phonon itself. In an experiment on ^{142}Nd [44] the strength of the branch to the 3^- state was found to be equal

within the error bars to the strength of the decay of the 2^+ phonon into the ground state, confirming the two-phonon character of the 1^- state in question. In our experiments, the decay of the 6027 keV level into the first 2^+ state is observed, but since it is impossible to disentangle the $E1$ and $E3$ strength involved in this transition, a conclusion cannot be drawn. The $E2$ transition from the decay into the 3^- phonon was not observed. Although very well investigated in heavier nuclei, information about this two-phonon state is rather sparse and its observation remains a challenge in the lighter nuclei.

The $E1$ strengths of the individual transitions can be compared with single particle estimates. For this, it is convenient to express the strengths in Weisskopf units (W.u.). The compilations of transition strengths by Endt, around 1980, provides us with an overview, presented in these single particle units, in different mass regions. On the basis of these compilations, a recommended upper limit (RUL) was deduced for different types of radiation in each mass region. For the $E1$ strength in the $A=45$–90 region, a RUL of 10 mW.u. was deduced [45]. At the time of the compilation, only two $E1$ transitions exceeding 1 mW.u. were known. In this report, however, no less than 18 (26 if strong transitions for which the parity is not known are included) new transitions exceeding 1 mW.u. are presented. The strongest transition in ^{56}Fe (^{58}Ni) has a strength of 5.85 (6.32) mW.u. These strengths do not exceed the RUL, but as all detected transitions are among the highest of the Endt compilation, it is probably safer to raise the RUL somewhat in this mass region.

The strongest $E1$ transition by far turned out to have practically the same excitation energy (8240 and 8237 keV) and strength (about $17\times10^{-3}e^2$ fm^2) in both nuclei. In ^{56}Fe it is accompanied by two somewhat smaller fragments. These almost exclusively account for the appearance of the strength concentration around 8.2 MeV. This remarkable feature also shows up in some neighboring fp-shell nuclei, measured mainly at the now dismantled NRF setup in Giessen. Figure 10 compares the oberved $E1$ transitions. In ^{54}Fe [9], the strongest $E1$ appears at 8.22 MeV with a $B(E1)\uparrow$ of $18.4\pm2.3\times10^{-3}e^2$ fm^2. Some smaller fragments appear at the low-energy side of this transition. For ^{52}Cr [46] the transition is shifted towards 7.90 MeV and has a strength of $25.1\pm9.1\times10^{-3}e^2$ fm^2. Since, as noted in Sec. III A, the strengths observed by Kumagai *et al.* [17] in the joint measurements on ^{56}Fe and ^{52}Cr are systematically too high, the strength for this transition was taken from a test experiment at the Mainz Microtron [47], in spite of its large error. If one takes note of the large error, the strength falls within the systematics of the other nuclei. The systematics seem broken in ^{60}Ni [9] and in ^{48}Ti [48], farther away from the closed shells. In ^{60}Ni, however, a transition, again of comparable strength ($18\pm2\times10^{-3}e^2$ fm^2), turns up at 9.6 MeV. This $E1$ strength concentration may be related to the so-called pygmy resonance observed in heavier nuclei, as already touched upon in the Introduction. In the $Z=50$ nuclei ^{116}Sn and ^{124}Sn [1] this resonance peaks at 6.4 MeV and at 6.5 MeV, respectively, with resonance strengths of 80 and 140 (upper limits of 120 and 180) $\times10^{-3}e^2$ fm^2. Analogous

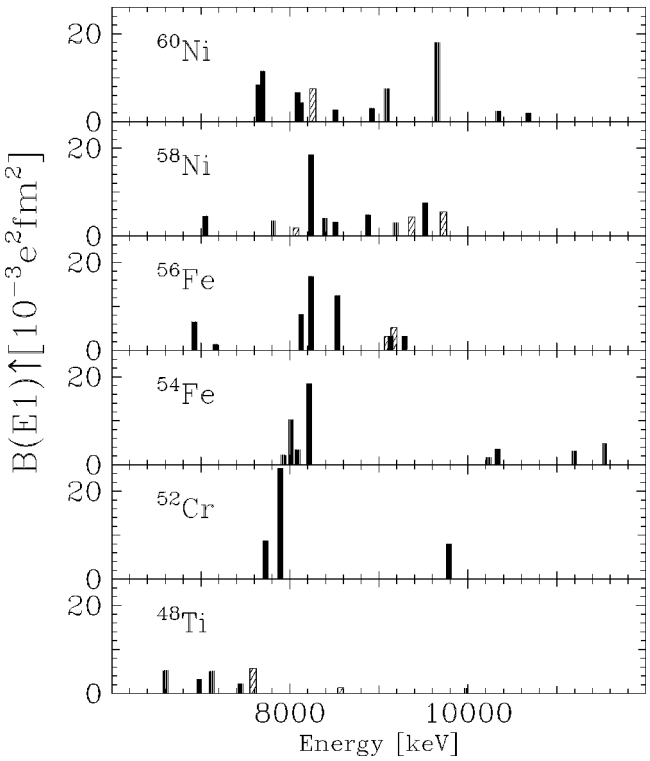

FIG. 10. Comparison of $E1$ transitions in several fp-shell nuclei. Hatched bars indicate tentative $E1$ assignments. See text for discussion.

resonances have been detected in (γ,γ') experiments on the $N=50$ nuclei ^{88}Sr, ^{89}Y, and ^{90}Zr (see Ref. [4] and references therein). For ^{88}Sr and ^{90}Zr strong transitions between 6 and 7 MeV were observed with a summed strength of about $80\times10^{-3}e^2$ fm^2. Only half of this strength was observed in ^{89}Y, but this is mainly due to the heavy fragmentation, expected in this odd nucleus, and to the fact that a maximum photon energy of 7 MeV was used, prohibiting observation of transitions close to this energy. In a recent NRF measurement in Gent on ^{92}Mo a double-humped structure between 6 and 7.4 MeV was observed, exhibiting a total $E1$ strength of $75\times10^{-3}e^2$ fm^2 [10]. The single transition in the fp shell could thus be regarded as such a less-fragmented resonance.

A possible explanation for this phenomenon considers the pygmy resonance as a leftover from the one phonon strength, which is pulled into the giant electric dipole resonance by residual interactions. Calculations performed within a two-group schematic RPA model on ^{116}Sn [11] showed that, besides the coherent mode (GDR) at higher energy, part of the $1p$-$1h$ strength remains trapped between the original $1p$-$1h$ states, giving rise to a series of smaller resonances. These local resonances can then be regarded as oscillations of a part of the nucleus against the nucleus bulk, in contrast to the GDR representing the full oscillating motion. From a collective point of view, these local resonances can be described as resulting from a local breaking of isospin symmetry [12,13]. Another theory is available, in which the oscillation of the neutron skin against the rest of the nucleus is responsible for the $E1$ strength concentrations on the tail of the GDR

[14,49]. In a recent heavy-ion experiment on Ca isotopes [50] this theory was investigated by comparing the $E1$ strength below the GDR in ^{40}Ca and ^{48}Ca. No strength difference between both nuclei was observed, providing no proof for the neutron skin theory, which predicts a much larger amount of $E1$ strength in ^{48}Ca due to the eight extra neutrons.

The QPM calculations do not reproduce accurately the resonance in ^{56}Fe or ^{58}Ni. It is possible that it can be connected with one of the strong resonances predicted by the QPM above 9 MeV. Another candidate for explaining theoretically the 8.2 MeV excitation could be the resonance predicted at about 7.6 MeV in both nuclei. In the QPM calculations this transition is mainly of one-phonon nature; it shows little fragmentation, and occurs in both nuclei at the same energy, as does the measured 8.2 MeV resonance.

B. $M1$ strength

The identified $M1$ transitions in ^{56}Fe and ^{58}Ni are displayed in Figs. 11(a) and 12(a), together with the smeared-out results (curve), using the same smearing parameter of 0.3 MeV as for the $E1$ transitions in the previous section. It is clear that, in contrast to the $E1$ strength, we deal here with a different behavior in both nuclei. In ^{56}Fe a strong low-lying $M1$ transition (scissors mode) of about $0.5\mu_N^2$ is present, and between 7 and 10 MeV there are some rather weak transitions ($\approx 0.2\mu_N^2$) spread over the energy region. In ^{58}Ni no noticeable $M1$ strength appears below 7 MeV. Between 7 and 10 MeV several transitions, roughly twice as strong as in ^{56}Fe, are the constituents of a resonance centered at 8.6 MeV. The total identified strength in this energy region is $(2.71 \pm 0.07)\mu_N^2$, while, in the same energy interval in ^{56}Fe, the identified $M1$ strength amounts to only $(1.37 \pm 0.12)\mu_N^2$.

In Figs. 11(b) and 12(b), all dipole transitions without parity assignments are added to the identified $M1$ transitions [similar as in Figs. 7(b) and 8(b)] to provide an upper limit for the $M1$ strength. As most of the low-lying transitions are probably $E2$ or inelastic transitions only the strength above 4 MeV is considered to determine an upper limit for the $M1$ strength (the 3448 keV transition in ^{56}Fe will be treated separately). For both nuclei the upper limit of the $M1$ strength amounts then to about $6.5\mu_N^2$. The real $M1$ strength is probably quite less, because most of the unidentified dipole transitions are likely to have an $E1$ character, building up the tail of the GDR (see also previous section). Even if the majority of these transitions would be $M1$, there is no evidence for a resonance in ^{56}Fe, similar to that in ^{58}Ni.

In a recent article by Nakada and Otsuka [51] a large-scale shell model calculation of the $B(M1)\uparrow$ distribution in ^{56}Fe is reported on. It places the centroids of the isospin conserving ($T=2$) and isospin raising ($T=3$) $M1$ strength well apart, respectively, at 9 and 18 MeV. In that paper, the results are presented in bins of 1 MeV. For the isospin conserving part a total strength of $B(M1)\uparrow = 12.7\mu_n^2$ was found, concentrated in a narrow resonance centered at 9.1 MeV and with significant tails down to 5 MeV and up to 12 MeV. It was also found that the orbital and spin parts of the interaction display a destructive interference within this energy region. Since only two active particles were considered, these calculations can provide no realistic reproduction of the fragmentation of the strength. Larger model spaces should be used, as in, e.g., Refs. [52,53]. In Ref. [53] shell model calculations were performed on, among others, ^{52}Cr and ^{54}Fe, allowing for four active particles. The fragmentation could be well reproduced and a quenching factor of $g_s^{eff} = 0.75 g_s^{free}$ was deduced. It appeared that the major part of the dramatic quenching predicted by previous calculations is mainly due to nuclear correlations, and meson exchange currents (MEC's) are thought to be of minor importance.

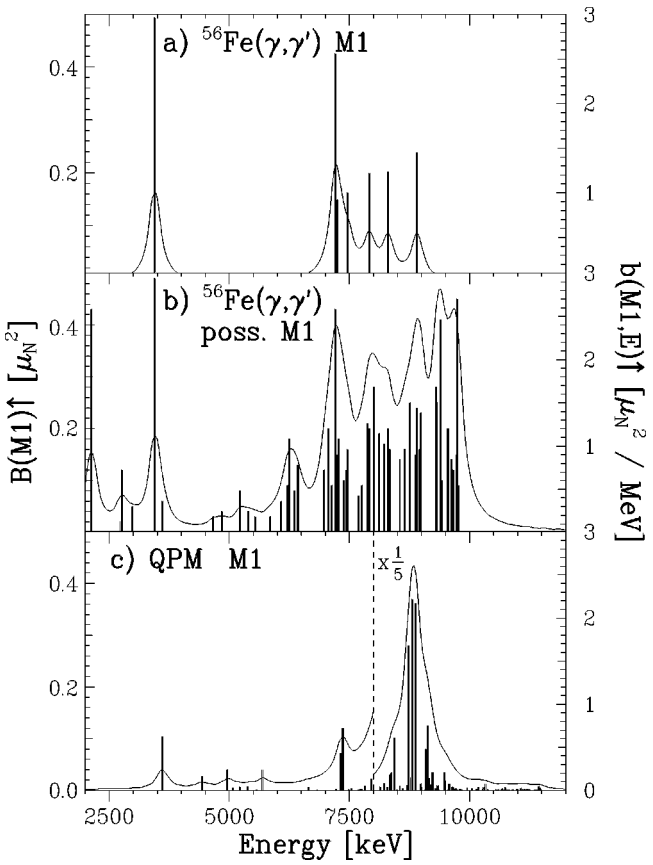

FIG. 11. $M1$ strength in ^{56}Fe from 2 to 12 MeV. Bars represent the individual transitions (left-hand scale). The curve (right-hand scale) represents the same results, but smeared out with a Breit-Wigner function with smearing parameter of 0.3 MeV. Part (a) displays transitions with an $M1$ assignment. In part (b) all observed transitions are included (including possible inelastic transitions), except those who could be identified as $E1$ or quadrupole. Transitions below 5 MeV (except the one at 3448 keV) are probably $E2$ or inelastic transitions, but are included for completeness. Part (c) displays the results of the QPM calculations.

As in our (γ,γ') measurements, in (e,e') [54] and (p,p') [55] experiments on ^{56}Fe the $M1$ strength was found to have a more or less flat distribution between 8 and 10 MeV. The strongest $M1$ detected in the (e,e') measurement (except for the 3448 keV transition) was the 7211 keV line which was also the strongest observed in our experiments.

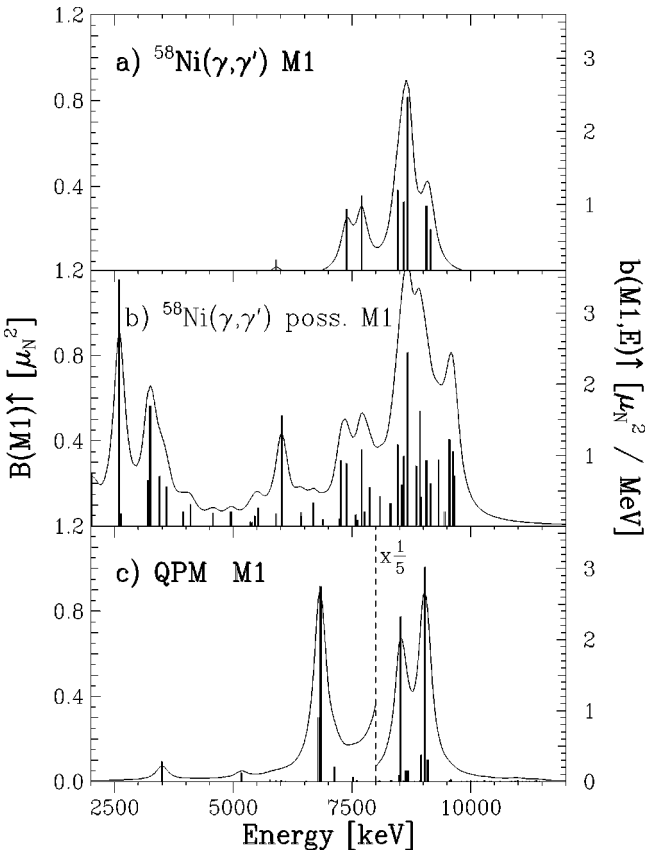

FIG. 12. The same as Fig. 11 but for ^{58}Ni.

The QPM calculations performed for the $M1$ strength in ^{56}Fe yield parallel but more detailed results than those from Ref. [51]. In the calculation of 1^+ excited states all one-phonon 1^+ configurations up to 15 MeV have been included in the wave function. In fact, there are only four of them in both nuclei. The number of two- and three-phonon configurations made up of phonons of different multipolarities which couple to 1^+, and are allowed by symmetry properties, is much larger. All of the two-phonon configurations with excitation energy below 14 MeV and three-phonon configurations made up of collective phonons have been included in the model space. The $B(M1)\uparrow$ values have been calculated using $g_s^{eff}=0.8g_s^{free}$. They are presented in Fig. 11(c), together with the smeared-out curve. Except for some weak transitions at lower energy, the bulk of the strength is comprised in a resonance, centered at 8.8 MeV and tailing out to about 8 and 10 MeV. The strength contained in this resonance is $9.9\mu_N^2$ while the total $M1$ strength from 4 to 10 MeV amounts to $10.2\mu_N^2$, an equivalent value to that from the shell model calculations [51].

Apparently there is not only a discrepancy between experimental and theoretical results in the shape of the $M1$ strength distribution but also in the amount of strength contained therein. Perhaps there is a larger amount of fragmentation than would theoretically be expected, resulting in a flatter distribution. Also, the deformation of ^{56}Fe, which was treated as a spherical nucleus in the present calculation, could perhaps influence the calculated strength and distribution.

In ^{58}Ni we do observe the expected resonance, centered at 8.6 MeV and with a total strength of $2.0\mu_N^2$ (and an upper limit of $4.6\mu_N^2$). The performed QPM calculations [Fig. 12(c)] reproduce this resonance as a double-humped structure formed mainly by two strong excitations at 8.5 and 9 MeV. For a complete agreement, the fragmentation is somewhat underestimated here. The calculated $M1$ strength, $11\mu_N^2$, for the resonance, however, exceeds several times the experimentally observed strength, just as in the case of ^{56}Fe. The calculations reveal also a smaller resonance ($1.3\mu_N^2$) centered at 6.8 MeV. Probably the transitions observed experimentally around 7.5 MeV can account for this: The observed strength ranges from $0.65\mu_N^2$ to $1.24\mu_N^2$ (upper limit) and is as such in good agreement if some fragmentation and a slight energy shift were applied to the calculated transitions.

Some ten years ago, electron scattering experiments were performed at the Darmstadt linear accelerator (DALINAC) in order to map the $M1$ strength distribution in ^{58}Ni from 6 to 15 MeV [15]. In the energy range overlapping the one studied in this report a rather similar behavior of the $M1$ strength can be found. There is a resonance between 8 and 9.5 MeV, containing $6.1\mu_N^2$ of $M1$ strength, and a smaller concentration around 7.5 MeV with a total strength of $1.5\mu_N^2$. The observed strengths are obviously higher than in the NRF experiments, rising even above the proposed upper limits. It is therefore necessary to make a more detailed comparison between the (e,e') and (γ,γ') results. Hereby, one has to bear in mind the different resolution of both methods [FWHM of about 30 keV in (e,e') and 7 keV at 7 MeV in (γ,γ')]. Of the twenty $M1$ transitions detected in (e,e'), seven can be confirmed as $M1$ transitions by the NRF results. Their strengths are in general in good agreement, except for the 7710 keV transition whose strength in NRF is only half of that in (e,e'), and for the 8680 keV transition for which our experiments yield twice the (e,e') strength. For the transition at 8962 keV, observed in the (e,e') experiment at 8967 keV, the present measurement provides no parity but only a dipole assignment. If analyzed as an $M1$ transition, its strength is quite small in comparison to the (e,e') result, so maybe it concerns two different transitions here. Eight further transitions have no equivalent in the NRF spectra, although they should lie above the detection limits in our experiments (except for two transitions very close to 10 MeV where the detection limits are not well known but are quite high).

More remarkable is the fact that five transitions (8237, 8514, 8880, 9369, and 9523 keV) in the (e,e') experiment, among which the two strongest, were identified as $E1$ transitions in the NRF experiments. If the $B(M1)\uparrow$ value from the (e,e') experiments is transformed to the level width Γ_0 through Eq. (2) and compared to the Γ_0 observed in NRF, the values agree within the error bars (except for the 8880 keV transition, which exceeds the NRF Γ_0 by a factor 3). Consequently there can be no accidental overlap of an $E1$ and $M1$ transition at virtually the same energy. Such an

overlap would also reduce the asymmetry measured in the polarized photon measurements, prohibiting a clear parity assignment. For the strongest transition at 8237 keV the measured asymmetry fitted perfectly the polarization degree (see Fig. 5), establishing without doubt the $E1$ character. It is also confirmed by a recent (p,p') experiment on ^{58}Ni performed at the RCNP (Osaka) with $E_p=160$ MeV and a scattering angle of 0° [56]. Preliminary results from the analysis reveals that the strongest peak appears at 8.68 MeV (also the strongest $M1$ transition in our experiments), while the peak heights of the peaks at 8.24 and 8.52 MeV are roughly half as large. If these five transitions are omitted from the comparison, the agreement in strength between the (e,e') and (γ,γ') results becomes better. For the strong resonance between 8 and 9.5 MeV, the (e,e') experiment yields now a strength of $3.2\mu_N^2$, in between the proposed lower and upper limit in NRF.

The results for ^{58}Ni are also confirmed qualitatively by the earlier proton scattering experiments by Djalali *et al.* [16]. However, no strength information is given in Ref. [16]. In the (p,p') spectrum an enhanced cross section is noticed between 6.4 and 10.5 MeV with two conspicuous peaks at 8.66 and 7.7 MeV. It must be mentioned that the two strongest transitions in the (e,e') experiments are not represented in the (p,p') spectra. Although the strongest peak at 8.66 MeV was considered as a possible $E1$ transition, the agreement with the (e,e') and NRF results is very good and the double-humped $M1$ structure is largely confirmed.

Besides the occurrence of $M1$ strength between 7 and 10 MeV, there remains a relatively large amount of strength at low energy in ^{56}Fe: the transition at 3448.6 keV, often referred to as a scissors mode [18,19,51]. In ^{58}Ni there is no evidence for such a strong low-energetic $M1$ transition. Its strength amounts to $(0.494\pm0.032)\mu_N^2$ and is the strongest $M1$ transition in the bound region in ^{56}Fe (the observed branching ratio of 0.79 ± 0.06 taken into account). The QPM calculations for ^{56}Fe yield a rather weak transition at 3607 keV ($0.10\mu_N^2$). Its structure is mainly a two-phonon mixed symmetry (MS) state, arising from the coupling of the first 2^+ phonon and the isovector MS 2^+ state ($2_1^+\otimes 2_{ms}^+$). A similar state was observed in NRF experiments on Te isotopes [57] and confirmed by QPM calculations. An analogy with the scissors mode was established. Also in ^{94}Mo the scissors mode was studied and its decay into the main component of the 2_{ms}^+ state clearly revealed its two-phonon MS character [58]. Apparently this should be a general feature of nearly spherical vibrational nuclei. The two-phonon structure implies a largely orbital character of this state. The discrepancy in strength for this ''scissors mode'' between experiment and QPM calculations is probably due to the fact that, in the present calculation, no deformation was introduced: apparently, the transition from the MS state to a spherical ground state is forbidden, but is enhanced by even a small deformation [51].

In the large-scale shell model calculations from Ref. [51] the connection between this 1^+ MS component and its transition strength to the ground state was investigated via the H^n cooling method. It turned out that the 1^+ MS component was distributed over two very close-lying shell model states (1_2^+ and 1_3^+) around 3.5 MeV. The mainly orbital character was also established. For these states, transition strengths of $B(M1)\uparrow=0.12\mu_N^2$ for the 1_2^+ state and $B(M1)\uparrow=0.30\mu_N^2$ for the 1_3^+ state were calculated. The summed strength comes close to the experimental value of $0.494\mu_N^2$. In the NRF experiment there is no indication of two components, however. The experimental strength value for this scissors mode agrees also quite well with that from the other two NRF experiments on ^{56}Fe [18,19], although it is somewhat overestimated in Ref. [19] because of the apparent presence of some feeding due to the higher end point energy (7.6 MeV) used there. In Ref. [18] the Γ_0^2/Γ value of the 3448.6 keV level is in agreement with our result, but a value of 0.5 for the branching ratio was used, resulting in a higher $B(M1)\uparrow$ value. The branching ratios from Ref. [19], from Ref. [34], and from our 6.5 MeV and 10 MeV end point energy measurements all agree within the error bars, however. In (e,e') experiments a $B(M1)\uparrow$ value of $(0.70\pm0.03)\mu_N^2$ was found for the orbital scissors mode [54].

The QPM calculations for ^{58}Ni predict a similar two-phonon MS state at 3500 keV, but there is no experimental evidence to support this. Unlike in ^{56}Fe, the absence of deformation prohibits an enhancement of the transition strength and consequently the observation of the transition strength or a proper spin-parity assignment.

C. Feeding and branching

It was already mentioned in previous sections that feeding of lower-lying levels by inelastic transitions from higher-lying levels poses a problem in NRF experiments and necessitates measurements at different end point energies of the bremsstrahlung. The source of this problem is the fact that in NRF experiments the deexcitation of levels is observed, in contrast to measurements with other probes like electrons and protons, where the direct excitation from the ground state is studied. Closely connected to the feeding problem is that of the branching of levels to states other than the ground state. Performing experiments at different end point energies can yield useful information about the feeding process, but branching can only be traced in a tentative way (via the Ritz rule) and only when the transitions to the ground state, to the intermediate state, and the transition of the intermediate state to the ground state are observed.

In ^{56}Fe we can estimate the amount of feeding by comparing the results from our 6.5 and 10 MeV experiments with those from the earlier 7.6 MeV experiment of Chapuran *et al.* [19]. It can be concluded that there is a certain, but not drastic, amount of feeding. Except for a high feeding of the 2133 keV transition, there is no real trend of dependence on the level energy noticeable in the feeding process.

In ^{58}Ni the situation is again more complex, due to the larger number of transitions present at low energy. The intensity of most of these seems to be not or only slightly increased by feeding. In contrast, two transitions at 2598 and 3254 keV show exceptionally large feeding. Since these were observed only in the 10 MeV experiment, it is likely that they have an inelastic origin. Again, as in ^{56}Fe, the

feeding shows no real dependence on the level energy, but is on the whole somewhat more important than in ^{56}Fe.

The feeding mechanism was studied in the framework of NRF measurements on Ge isotopes by means of statistical calculations [23]. The main conclusion was that feeding (primary and secondary feeding included) is most probable from states which are about 2–3 MeV above the level being fed. Consequently, when using 10 MeV bremsstrahlung, only for energies below 6 MeV does feeding becomes noticeable and below 4 MeV drastic. However, for this statement no conclusive evidence can be found in ^{56}Fe or ^{58}Ni, as stated above.

The γ peak due to the deexcitation of the first 2^+ state in both nuclei (847 and 1454 keV for ^{56}Fe and ^{58}Ni, respectively) is very conspicuous in the spectra, indicating a large amount of feeding. This large population of both 2^+ states can only for a small part be accounted for by the observed inelastic transitions to these states. Furthermore, most of the observed feeding in our experiments of the levels between 2 and 6 MeV cannot be connected with the observed branching in both nuclei. Two suggestions can be brought forward: First, the shortage of suitable inelastic transitions may point at a feeding mechanism consisting of many weak inelastic transitions, which fall below the detection limits. Second, the presence of some strong low-energetic transitions, suspected of being unidentified inelastic transitions (certainly in ^{58}Ni), leads to the possibility that for certain levels branching exhausts the strength so heavily that the decay to the ground state is not visible anymore in the spectrum. Consequently the Ritz rule can give no indication for a possible inelastic nature.

Arguments for these suggestions can be found in the tagged photon experiments on ^{56}Fe by Chapuran *et al.* [19]. The differential cross section for inelastic photon scattering, leaving ^{56}Fe in the first 2^+ state at 847 keV, was found to be generally about half as large as the elastic cross section. It shows no structure and has a rather flat distribution up to 10 MeV. Apparently this cross section is the result of the cumulative effect of many levels branching weakly to the 2_1^+ state. The branching is thus certainly more important than observed in the NRF experiments. Also comparing the results for the $M1$ transitions with those from electron scattering experiments [15,54] provides evidence for this branching. Although these (e,e') experiments have detection limits comparable to those in NRF, several $M1$ transitions that have a strength lying above the detection limits are not observed in the NRF measurements. Strong branching of some of these 1^+ states seems consequently the cause of this observation. It is, however, in contrast to a simplified QPM calculation in which the branching of pure one-phonon 1^+ states into intermediate one- and two-phonon states is considered. Since $E1$ decays are predominant, the states with $J^\pi=0^-$, 1^-, and 2^- are accounted for as intermediate ones. This results in a very weak branching, affecting the ground state $M1$ transition only within 1%. Most of the branching and feeding must consequently originate from 1^-, and not from 1^+ states. This is obvious, as there are more 2^+ states at low energy, suitable for being populated via $E1$ transitions, than 0^-,1^-,2^- states.

In conlusion, feeding and to a greater extent branching of levels, remains a problem in NRF studies and prevents in some cases an accurate determination of transition strengths.

V. CONCLUSIONS

A high-resolution study of the fp-shell nuclei ^{56}Fe and ^{58}Ni for excitation energies between 2 and 10 MeV was performed at the 15 MeV linac in Gent by means of resonant scattering of bremsstrahlung photons. The fine structure of the dipole strength in this energy region was obtained for each nucleus. Two runs with different bremsstrahlung end point energy were done in order to account for feeding effects. Experiments with partially linearly polarized bremsstrahlung enabled the determination of parities for the strongest transitions in a model-independent way. In each nucleus more than 60 transitions were observed. Excitation energies and ground state transition widths were determined. For some states, branching was detected via the Ritz rule and their ground state transition widths were recalculated accordingly. These results were compared with earlier, less complete, NRF experiments on these nuclei.

In the two nuclei together, reduced transition probabilities for 20 $E1$ and 15 $M1$ transitions could be determined. The strongest transitions turned out to have an $E1$ character. The main $E1$ strength lies between 5 and 10 MeV and amounts to about $60\times10^{-3}e^2$ fm^2 (with an upper limit of $140\times10^{-3}e^2$ fm^2) in this energy region. The $E1$ strength distribution shows a narrow concentration around 8.2 MeV, consisting of only a few strong transitions. The strongest transition by far has the same excitation energy and strength in both nuclei. Arguments were given to consider this resonance as analogous to the $E1$ pygmy resonance observed in heavier nuclei. Calculations in the framework of the QPM model were performed for the $E1$ as well as the $M1$ strength in these nuclei. For the $E1$ strength there is no one-to-one corrrespondence with the experiments, but the overall strength between 5 and 10 MeV is in fair agreement. The majority of the strong $E1$ QPM transitions appears above 10 MeV. The strong 8.2 MeV resonance is not reproduced quite well, but some candidates in the calculations can be brought forward.

In ^{58}Ni, the QPM calculations predict also a $|2_1^+\otimes3_1^-;1^-\rangle$ two-phonon state at 5800 keV. The observed dipole transition at 6027 keV is a good candidate, having the same strength ($6\times10^{-3}e^2$ fm^2) but unfortunately no parity asignment.

In contrast to the $E1$ strength, the $M1$ strength shows a different behavior in the two nuclei. Only in ^{56}Fe a strong $M1$ transition at low energy appears (3.5 MeV) with an $M1$ strength of about $0.5\mu_N^2$. The QPM calculations confirm the two-phonon mixed-symmetry structure ($|2_1^+\otimes2_{ms}^+;1^+\rangle$), which has a mainly orbital character. In ^{58}Ni the QPM calculations also predict such a 1^+ state, but its strength is probably too small to be detectable.

The $M1$ strength in ^{56}Fe at higher energies shows a rather flat distribution between 7 and 9 MeV with a total $M1$ strength between $1.4\mu_N^2$ and $6.5\mu_N^2$. The QPM calculations

predict a narrow resonance around 9 MeV, where the spin-flip strength is indeed expected. Its strength is rather overestimated compared to the NRF observations, reaching $10\mu_N^2$. In the $M1$ strength distribution in ^{58}Ni this resonance is present, however, centered around around 8.7 MeV and exhibiting an $M1$ strength between $2.0\mu_N^2$ and $4.6\mu_N^2$. The QPM calculations indeed predict a resonance between 8 and 9.5 MeV. The strength, however, is again rather overestimated $(11\mu_N^2)$.

By comparing the results from the experiments at different bremsstrahlung end point energies, a study of the feeding of low-lying levels could be performed. It turned out that only below 6 MeV excitation energy feeding becomes noticeable, but exhibits no real dependence on the energy. It appears that only for the first 2^+ state does feeding take drastic forms. Inelastic transitions, responsible for this feeding, could only in a few cases be identified, implicating that feeding proceeds mainly via many weak inelastic transitions, which individually fall below the detection limits of the experiments. A second explanation for the shortage of identified inelastic transitions supposes that branching of some levels is so drastic that the decay to the ground state becomes too weak to be observed and the possibility of identifying the inelastic transitions vanishes. This mechanism is supported by the observation of certain strong low-lying transitions, which show characteristics of being inelastic but cannot be identified as such. Also, for the $M1$ transitions, this could account for the discrepancies between NRF and (e,e') results, although a simple calculation in the QPM model predicts the branching of 1^+ levels to be very small.

ACKNOWLEDGMENTS

We want to thank the technical staff of the Nuclear Physics Laboratory in Gent for the reliable operation of the linac during our experiments. We also thank K. Huber and R. Stock for their help with the experimental setup. To Professor K. Heyde, Professor Iachello, Dr. P. Von Neumann-Cosel, and Dr. C. De Coster we are greatly indebted for their suggestions and enlightening dicussions. This work is part of the research program of the Fund for Scientific Research Flanders. V.Y.P. acknowledges support from the Research Council of the University of Gent and NATO.

[1] K. Govaert, F. Bauwens, J. Bryssinck, D. De Frenne, E. Jacobs, W. Mondelaers, L. Govor, and V. Yu. Ponomarev, Phys. Rev. C **57**, 2229 (1998).

[2] R.-D. Herzberg, C. Fransen, P. von Brentano, J. Eberth, J. Enders, A. Fitzler, L. Käubler, H. Kaiser, P. von Neumann-Cosel, N. Pietralla, V. Yu. Ponomarev, H. Prade, A. Richter, H. Schnare, R. Schwengner, S. Skoda, H. G. Thomas, H. Tiesler, D. Weisshaar, and I. Wiedenhöver, Phys. Rev. C **60**, 051307(R) (1999).

[3] R.-D. Herzberg, P. von Brentano, J. Eberth, J. Enders, R. Fischer, N. Huxel, T. Klemme, P. von Neumann-Cosel, N. Nicolay, N. Pietralla, V. Yu. Ponomarev, J. Reif, A. Richter, C. Schlegel, R. Schwengner, S. Skoda, H. G. Thomas, I. Wiedenhöver, G. Winter, and A. Zilges, Phys. Lett. B **390**, 49 (1997).

[4] J. Reif, P. von Brentano, J. Eberth, J. Enders, R.-D. Herzberg, N. Huxel, L. Kaübler, P. von Neumann-Cosel, N. Nicolay, N. Pietralla, H. Prade, A. Richter, C. Schlegel, H. Schnare, R. Schwenger, T. Servene, S. Skoda, H. G. Thomas, I. Wiedenhöver, G. Winter, and A. Zilges, Nucl. Phys. **A620**, 1 (1997).

[5] R. M. Laszewski and P. Axel, Phys. Rev. C **19**, 342 (1979).

[6] R. M. Laszewski, Phys. Rev. C **34**, 1114 (1986).

[7] L. Cannel, Ph.D. thesis, University Illinois, 1976.

[8] K. Wienhard, C. Bläsing, K. Ackermann, K. Bangert, U. E. P. Berg, K. Kobras, W. Naatz, D. Rück, R. K. M. Schneider, and R. Stock, Z. Phys. A **302**, 185 (1981).

[9] U. E. P. Berg, Habilitation thesis, University Giessen, 1985.

[10] F. Bauwens, J. Bryssinck, D. De Frenne, K. Govaert, L. Govor, M. Hagemann, J. Heyse, E. Jacobs, W. Mondelaers, and V. Yu. Ponomarev, in Abstracts of the General Scientfic Meeting of the Belgian Physical Society, VUB Brussels, 1999, p. NP8.

[11] A. Oros, K. Heyde, C. De Coster, and B. Decroix, Phys. Rev. C **57**, 990 (1998).

[12] F. Iachello, private communication and workshop on low-lying dipole excitations in Darmstadt, 1997.

[13] F. Iachello, Phys. Lett. **160B**, 1 (1985).

[14] P. Van Isacker, M. A. Nagarajan, and D. D. Warner, Phys. Rev. C **45**, R13 (1992).

[15] W. Mettner, A. Richter, W. Stock, B. C. Metsch, and A. G. M. Van Hees, Nucl. Phys. **A473**, 160 (1987).

[16] C. Djalali, N. Marty, M. Morlet, A. Willis, J. C. Jourdain, N. Anantaraman, G. M. Crawley, A. Galonsky, and P. Kitching, Nucl. Phys. **A388**, 1 (1982).

[17] N. Kumagai, T. Ishimatsu, E. Tanaka, K. Kageyama, and G. Isoyama, Nucl. Phys. **A329**, 205 (1979).

[18] B. S. Ishkanov, I. M. Kapitonov, A. Y. Ugaste, V. I. Shvedunov, and E. V. Shirokov, Phys. At. Nucl. **57**, 2041 (1994).

[19] T. Chapuran, R. Starr, R. Vodhanel, and M. K. Brussel, Phys. Rev. C **30**, 54 (1984).

[20] K. Govaert, W. Mondelaers, E. Jacobs, D. De Frenne, K. Persyn, S. Pommé, M. L. Yoneama, S. Lindenstruth, K. Huber, A. Jung, B. Starck, R. Stock, C. Wesselborg, R. D. Heil, U. Kneissl, and H. H. Pitz, Nucl. Instrum. Methods Phys. Res. A **337**, 265 (1994).

[21] K. Ackerman, K. Bangert, U. E. P. Berg, G. Junghans, R. K. M. Schneider, R. Stock, and K. Wienhard, Nucl. Phys. **A372**, 1 (1981).

[22] C. Bläsing, Ph.D. thesis, University Giessen, 1982.

[23] A. Jung, S. Lindenstruth, H. Schacht, B. Starck, R. Stock, C. Wesselborg, R. D. Heil, U. Kneissl, J. Margraf, H. H. Pitz, and F. Steiper, Nucl. Phys. **A584**, 103 (1995).

[24] S. Skorka, in *The Electromagnetic Interaction in Nuclear Spectroscopy*, edited by W. Hamilton (North-Holland, Amsterdam, 1975), p. 283.

[25] F. R. Metzger, Prog. Nucl. Phys. **7**, 53 (1959).

[26] U. Kneissl, H. H. Pitz, and A. Zilges, Prog. Part. Nucl. Phys. **37**, 349 (1996).
[27] L. W. Fagg and S. S. Hanna, Rev. Mod. Phys. **31**, 711 (1959).
[28] F. Ajzenberg-Selove, Nucl. Phys. **A433**, 1 (1985).
[29] F. Ajzenberg-Selove, Nucl. Phys. **A460**, 20 (1986).
[30] L. I. Schiff, Phys. Rev. **83**, 252 (1951).
[31] H. Junde, H. Dailing, Z. Chunmei, H. Xiaoling, H. Baohua, and W. Yaodong, Nucl. Data Sheets **51**, 1 (1987).
[32] B. Singh, Nucl. Data Sheets **62**, 603 (1991).
[33] P. B. Smith and W. Segeth, Nucl. Phys. **A398**, 397 (1982).
[34] B. S. Ishkanov, I. M. Kapitonov, E. V. Shirokov, B. A. Yur'ev, L. I. Govor, A. M. Demidov, and O. K. Zhuravlev, Phys. At. Nucl. **61**, 515 (1998).
[35] M. R. Bhat, Nucl. Data Sheets **80**, 789 (1997).
[36] V. Yu. Ponomarev and P. von Neumann-Cosel, Phys. Rev. Lett. **82**, 501 (1999).
[37] V. Yu. Ponomarev, J. Bryssinck, L. Govor, F. Bauwens, O. Beck, D. Belic, P. von Brentano, D. De Frenne, C. Fransen, R.-D. Herzberg, E. Jacobs, U. Kneissl, H. Maser, A. Nord, N. Pietralla, H. H. Pitz, and V. Werner, Phys. Rev. Lett. **83**, 4029 (1999).
[38] S. K. Patra and C. R. Praharaj, Phys. Rev. C **44**, 2552 (1991).
[39] G. Scharff-Goldhaber and C. B. Dover, Annu. Rev. Nucl. Part. Sci. **26**, 239 (1976).
[40] F. Ballester, E. Casal, and J. B. A. England, Nucl. Phys. **A501**, 301 (1989).
[41] J. Bryssinck, L. Govor, D. Belic, F. Bauwens, O. Beck, P. von Brentano, D. De Frenne, T. Eckert, C. Fransen, K. Govaert, R.-D. Herzberg, E. Jacobs, U. Kneissl, H. Maser, A. Nord, N. Pietralla, H. H. Pitz, V. Yu. Ponomarev, and V. Werner, Phys. Rev. C **59**, 1930 (1999).
[42] T. Eckert, O. Beck, J. Besserer, P. von Brentano, R. Fischer, R.-D. Herzberg, U. Kneissl, J. Margraf, H. Maser, A. Nord, N. Pietralla, H. H. Pitz, S. W. Yates, and A. Zilges, Phys. Rev. C **56**, 1256 (1997).
[43] R.-D. Herzberg, I. Bauske, P. von Brentano, T. Eckert, R. Fischer, W. Geiger, U. Kneissl, J. Margraf, H. Maser, N. Pietralla, H. H. Pitz, and A. Zilges, Nucl. Phys. **A592**, 211 (1995).
[44] M. Wilhelm, S. Kasemann, G. Pascovici, E. Radermacher, P. von Brentano, and A. Zilges, Phys. Rev. C **57**, 577 (1998).
[45] P. M. Endt, At. Data Nucl. Data Tables **23**, 547 (1979).
[46] U. E. P. Berg, D. Rück, K. Ackermann, K. Bangert, C. Bläsing, K. Kobras, W. Naatz, R. K. M. Schneider, R. Stock, and K. Wienhard, Phys. Lett. **103B**, 301 (1981).
[47] D. Rück, Diploma thesis, Insititut für Kernphysik, Giessen, 1982.
[48] A. Degener, C. Bläsing, R. D. Heil, A. Jung, U. Kneissl, H. H. Pitz, H. Schacht, S. Schennach, R. Stock, and C. Wesselborg, Nucl. Phys. **A513**, 29 (1990).
[49] J. Chambers, E. Zaremba, J. P. Adams, and B. Castel, Phys. Rev. C **50**, R2671 (1994).
[50] S. Ottini-Hustache, N. Alamanos, F. Auger, B. Castel, Y. Blumenfeld, V. Chiste, N. Frascaria, A. Gillibert, C. Jouanne, V. Lapoux, F. Marie, W. Mittig, J. C. Roynette, and J. A. Scarpaci, Phys. Rev. C **59**, 3429 (1999).
[51] H. Nakada and T. Otsuka, Phys. Rev. C **55**, 2418 (1997).
[52] E. Caurier, A. Poves, and A. P. Zuker, Phys. Rev. Lett. **74**, 1517 (1995).
[53] P. von Neumann-Cosel, A. Poves, J. Retamosa, and A. Richter, Phys. Lett. B **443**, 1 (1998).
[54] G. Hartung, Diploma thesis, Technische Hochschule Darmstadt, 1989.
[55] A. Richter, in *Proceedings of the 4th International Spring Seminar on Nuclear Physics: The Building Blocks of Nuclear Structure*, edited by A. Covello (World Scientific, Singapore, 1992), p. 335.
[56] Y. Fujita (private communication).
[57] R. Schwenger, G. Winter, W. Schauer, M. Grinberg, F. Becker, P. von Brentano, J. Eberth, J. Enders, T. von Egidy, R.-D. Herzberg, N. Huxel, L. Kaübler, P. von Neumann-Cosel, N. Nicolay, J. Ott, N. Pietralla, H. Prade, S. Raman, J. Reif, A. Richter, C. Shlegel, H. Schnare, T. Servene, S. Skoda, T. Steinhardt, C. Stoyanov, H. G. Thomas, I. Wiedenhöver, and A. Zilges, Nucl. Phys. **A620**, 77 (1997).
[58] N. Pietralla, C. Fransen, D. Belic, P. von Brentano, C. Friessner, U. Kneissl, A. Linneman, A. Nord, H. H. Pitz, T. Otsuka, I. Schneider, V. Werner, and I. Wiedenhoöver, Phys. Rev. Lett. **83**, 1303 (1999).